Ages and metallicities of early-type galaxies in the Sloan Digital Sky Survey: new insight into the physical origin of the colour-magnitude and the Mg2-σV relations

Anna Gallazzi, Stéphane Charlot, Jarle Brinchmann, Simon D. M. White

Mon. Not. R. Astron. Soc. **370,** 1106–1124 (2006) doi:10.1111/j.1365-2966.2006.10548.x

Ages and metallicities of early-type galaxies in the Sloan Digital Sky Survey: new insight into the physical origin of the colour–magnitude and the Mg_2–σ_V relations

Anna Gallazzi,[1]⋆ Stéphane Charlot,[1,2] Jarle Brinchmann[3] and Simon D. M. White[1]

[1]*Max-Planck-Institut für Astrophysik, Karl-Schwarzschild-Str. 1, D-85748 Garching bei München, Germany*
[2]*Institut d'Astrophysique de Paris, UMR7095 CNRS, Université Pierre & Marie Curie, 98 bis boulevard Arago, 75014 Paris, France*
[3]*Centro de Astrofísica da Universidade do Porto, Rua das Estrelas – 4150-762 Porto, Portugal*

Accepted 2006 May 11. Received 2006 May 10; in original form 2005 December 22

ABSTRACT

We exploit recent constraints on the ages and metallicities of early-type galaxies in the Sloan Digital Sky Survey (SDSS) to gain new insight into the physical origin of two fundamental relations obeyed by these galaxies: the colour–magnitude and the Mg_2–σ_V relations. Our sample consists of 26 003 galaxies selected from the SDSS Data Release 2 (DR2) on the basis of their concentrated light profiles, for which we have previously derived median-likelihood estimates of stellar metallicity, light-weighted age and stellar mass. Our analysis provides the most unambiguous demonstration to date of the fact that both the colour–magnitude and the Mg_2–σ_V relations are primarily sequences in stellar mass and that total stellar metallicity, α-elements-to-iron abundance ratio and light-weighted age all increase with mass along the two relations. For high-mass ellipticals, the dispersion in age is small and consistent with the error. At the low-mass end, there is a tail towards younger ages, which dominates the scatter in colour and index strength at fixed mass. A small, but detectable, intrinsic scatter in the mass–metallicity relation also contributes to the scatter in the two observational scaling relations, even at high masses. Our results suggest that the chemical composition of an early-type galaxy is more tightly related to its dynamical mass (including stars and dark matter) than to its stellar mass. The ratio between stellar mass and dynamical mass appears to decrease from the least massive to the most massive galaxies in our sample.

Key words: galaxies: evolution – galaxies: formation – galaxies: stellar content.

1 INTRODUCTION

The observed properties of early-type galaxies obey several fundamental relations, which have long been thought to hide important clues about the physical processes that influenced the formation and evolution of these galaxies. For example, luminosity, central velocity dispersion σ_V, mean surface brightness, brightness profile, colours and Mg_2 absorption-line index all appear to be tightly related to each other in early-type galaxies (Baum 1959; Faber & Jackson 1976; Kormendy 1977; Visvanathan & Sandage 1977; Djorgovski & Davis 1987; Bender, Burstein & Faber 1993). The colour–magnitude and the Mg_2–σ_V relations are particularly interesting in that they connect the luminous and dynamical masses of the galaxies with the physical properties of their stellar populations. The tightness and homogeneity of these two relations must be telling us something fundamental about the epoch and the process of formation of early-type galaxies (see for a review Renzini 2006).

⋆E-mail: gallazzi@MPA-Garching.MPG.DE

The physical interpretation of the above observational relations is still a subject of debate. The colour–magnitude relation (CMR) is often interpreted as a sequence of increasing metallicity with increasing luminosity (Faber 1973; Worthey 1994; Kodama & Arimoto 1997; Kodama, Bower & Bell 1999). However, it has been proposed that, in addition to metallicity, age could at least in part drive the relation (Gonzalez, Faber & Worthey 1993; Ferreras, Charlot & Silk 1999; Terlevich et al. 1999; Poggianti et al. 2001a). Studies of evolution with cosmic time indicate that the slope of the CMR has changed little since $z \sim 1$ (Kodama & Arimoto 1997; Kodama et al. 1998; Stanford, Eisenhardt & Dickinson 1998; Blakeslee et al. 2003). This has been used as an argument against age as the primary driver of the relation, since the colours of young stellar populations evolve faster than those of old stellar populations. Similar interpretations have been proposed for the relation between Mg_2 index strength and central velocity dispersion σ_V, which is generally thought to arise from a combination of age and metallicity variations (Colless et al. 1999; Trager et al. 2000a; Kuntschner et al. 2001).

The difficulty of obtaining unambiguous constraints on the relative influence of age and metallicity on the colour–magnitude and

the Mg_2–σ_V relations is a consequence of the difficulty of deriving accurate ages and metallicities for large samples of early-type galaxies: age and metallicity both tend to redden the colours and strengthen the Mg_2 absorption line in similar ways (e.g. Worthey 1994). In addition, at fixed metallicity, the α-element-to-iron (α/Fe) abundance ratio appears to be larger in the most massive early-type galaxies than in the nearby stars used to calibrate age and metallicity estimates (Worthey, Faber & Gonzalez 1992; Vazdekis et al. 2001). This has been explored recently by Thomas, Maraston & Korn (2004), who used 'closed-box' chemical evolution models with variable heavy-element abundance ratios to analyse a heterogeneous sample of 124 nearby early-type galaxies, in both low- and high-density environments. According to these models, massive galaxies formed earlier and more rapidly than low-mass galaxies, while both the colour–magnitude and the Mg_2–σ_V relations are primarily driven by metallicity. Bernardi et al. (2003a,b,c,d) carried out a more observationally oriented analysis on a sample of nearly 9000 early-type galaxies from the Sloan Digital Sky Survey (SDSS). They showed that the CMR reflects a dependence of both colour and luminosity on velocity dispersion. By *assuming* that luminosity traces metallicity and that the scatter in colour at fixed luminosity traces age, Bernardi et al. (2005) explored how age and metallicity may be related to velocity dispersion in early-type galaxies.

In this paper, we re-examine the physical origin of the colour–magnitude and the Mg_2–σ_V relations using a different approach. Our starting point is a set of statistical estimates of light-weighted age, stellar metallicity and stellar mass for a large sample of 26 003 early-type galaxies drawn from the SDSS Data Release 2 (DR2). We derived these constraints in earlier work by using a comprehensive library of model spectra at medium–high resolution (Gallazzi et al. 2005, hereafter Paper I) to interpret the strengths of five spectral absorption features with negligible dependence on the α/Fe ratio. We use here this data set, together with an observational tracer of the α/Fe ratio, to demonstrate unambiguously that both the colour–magnitude and the Mg_2–σ_V relations of early-type galaxies are primarily sequences in stellar mass and that both the total stellar metallicity and the α/Fe ratio increase with mass along the two relations. Light-weighted age increases from the least massive to the most massive early-type galaxies, with a larger spread at low masses that dominates the scatter in the colour–magnitude and Mg_2–σ_V relations. The small intrinsic scatter in metallicity at fixed mass also contributes to the scatter in the two scaling relations.

We present our sample in Section 2, along with a brief description of the method adopted in Paper I to derive statistical estimates of the ages, metallicities and stellar masses of the galaxies. The influence of these parameters on the colour–magnitude and the Mg_2–σ_V relations is explored in Sections 3.1 and 3.2, respectively, and their possible dependence on galaxy environment is addressed in Section 3.3. In Section 3.4, we discuss some implications on the relations between physical parameters and dynamical mass. Section 4 summarizes our conclusions. Throughout the paper, we use $\Omega_m = 0.3, \Omega_\Lambda = 0.7$ and $H_0 = 70\,km\,s^{-1}\,Mpc^{-1}$.

2 OBSERVATIONAL SAMPLE

We select our sample from the main spectroscopic sample of the SDSS DR2 (Abazajian et al. 2004). The SDSS is an imaging and spectroscopic survey of the high Galactic latitude sky, which will obtain u, g, r, i and z photometry of almost a quarter of the sky and spectra of at least 700 000 objects (York et al. 2000). The spectra are taken using 3-arcsec diameter fibres, positioned as close as possible to the centres of the target galaxies. Stellar metallicity, light-weighted age and stellar mass estimates are available from Paper I for a sample of 175 128 galaxies with Petrosian r-band magnitudes in the range $14.5 < r < 17.77$ (after correction for foreground Galactic extinction) and in the redshift range $0.005 < z \leqslant 0.22$. The lower redshift limit allows us to include low-luminosity galaxies (corresponding to a stellar mass of $\sim 10^8\,M_\odot$), while still avoiding redshifts for which deviations from the Hubble flow can be substantial. The upper limit corresponds roughly to the redshift at which a typical $10^{11}\,M_\odot$ galaxy is detected with median signal-to-noise ratio (S/N) per pixel greater than 20.

We select early-type galaxies on the basis of the light concentration index $C = R_{90}/R_{50}$, defined as the ratio of the radii enclosing 90 and 50 per cent of the total Petrosian r-band luminosity of a galaxy. This parameter has been shown to correlate well with morphological type (Shimasaku et al. 2001; Strateva et al. 2001). Thus, it allows a rough morphological classification of SDSS galaxies. Strateva et al. (2001) propose a cut at $C = 2.6$ to separate early- from late-type galaxies. To limit the contamination by disc galaxies with large bulges, we define here as 'early type' those galaxies with concentration index $C \geqslant 2.8$. In this way, we select 67 411 early-type galaxies in the redshift range $0.005 < z \leqslant 0.22$. We note that we decided against further limiting the contamination of our sample by systems with residual star formation by imposing a lower cut-off in 4000-Å break strength or an upper limit on emission lines equivalent width. Since these quantities correlate with colour, such limits would introduce an unwanted cut-off in the CMR.[1]

Bayesian-likelihood estimates of the r-band light-weighted ages, stellar metallicities and stellar masses of the 67 411 galaxies in our sample are available from Paper I. These estimates were derived by comparing the spectrum of each galaxy to a library of Bruzual & Charlot (2003) models at medium–high spectral resolution, encompassing the full range of physically plausible star formation histories. In practice, we compared the strengths of five spectral absorption features in the spectrum of each observed galaxy to the strengths of these features in every model spectrum (broadened to the observed velocity dispersion) in the library. We used D4000, Hβ and Hδ_A+Hγ_A as age-sensitive indices and [Mg_2Fe] and [MgFe]′ as metal-sensitive indices, all of which depend negligibly on the α/Fe ratio.[2] This comparison allowed us to construct the probability density functions of age, metallicity and stellar mass for every galaxy. The estimate of each parameter is given by the median of the corresponding probability distribution, while the $\pm 1\sigma$ error on each parameter is given by half the 16–84 per cent percentile range of the likelihood distribution (this would be equivalent to the $\pm 1\sigma$ range for a Gaussian distribution).

We note that the stellar ages, as well as the other physical parameters, are derived by fitting the galaxy spectra as observed and so refer to the galaxies at the time they are observed. Because of the bright and faint magnitude limits in our sample, there is a strong correlation between luminosity and redshift. If uncorrected, it may

[1] Bernardi et al. (2005) adopted a different criterion to select early-type galaxies from the SDSS. They considered to be of early type those galaxies for which the r-band surface brightness profile is better described by a de Vaucouleurs law than by an exponential law (photometric parameter fracDev > 0.8) and that do not have emission lines (spectroscopic parameter eclass < 0).

[2] This might not be entirely correct for Hδ_A and Hγ_A, which are suspected to depend on the α/Fe ratio at high metallicity (Thomas et al. 2004; Korn, Maraston & Thomas 2005). However, we did not find any discrepancy between the metallicities and ages derived including or excluding Hδ_A+Hγ_A (see section 2.4.2 of Paper I).

introduce systematic effects in correlations between age and luminosity (or mass). To avoid this, we correct our measured ages so that they are relative to the present, rather than to the point of observation, by adding to the measured age for each galaxy the look-back time to the redshift at which it is observed. The metallicity is left unchanged. This look-back time varies from 0.07 to 2.64 Gyr over the redshift range covered by our sample. The corrections mainly affect the most luminous galaxies, which are found out to higher redshifts. All light-weighted ages quoted throughout this paper refer to $z = 0$.

As described in Paper I, our constraints on metallicity and age are sensitive to the observational signal-to-noise ratio (S/N) of the spectra. A median S/N per pixel of at least 20 is required to constrain metallicity reliably. For this reason, here we consider only those galaxies with a median S/N per pixel greater than 20. This cut reduces our sample to 26 003 high-concentration galaxies in the redshift range $0.005 < z \leqslant 0.22$. This is the same sample of 'early-type' galaxies as analysed in section 3.3 of Paper I. As shown there, the S/N requirement biases the sample towards low-redshift, high-surface brightness galaxies, but it does not introduce any bias in the luminosity, colour, velocity dispersion and index-strength distributions of the early-type galaxy sample.

Our selection of early-type galaxies, based only on the concentration parameter, includes early-type spiral galaxies, galaxies with emission lines and active galactic nuclei (AGN). We can divide our sample into five subclasses according to the classification given by Brinchmann et al. (2004) on the basis of the emission-line properties of SDSS DR2 galaxies. Following their notation, we label as (i) unclassifiable ('Unclass.') those galaxies which cannot be classified using the Baldwin, Phillips & Terlevich (1981) diagram, i.e. mostly galaxies with no or weak emission lines; (ii) AGN those galaxies with a substantial AGN contribution to their emission-line fluxes; (iii) star forming ('SF') those galaxies with S/N > 3 in Hβ, Hα, [O III]5007, [N II]6564 emission lines and for which the contribution to Hα from AGN is less than 1 per cent; (iv) composite ('C') those galaxies with S/N>3 in the same four lines, but for which the AGN contribution to Hα luminosity can be up to 40 per cent; (v) low-S/N star forming ('low-S/N SF') those galaxies with S/N > 2 in Hα but without AGN contribution to their spectra. The sample includes 10 982 unclassifiable galaxies, 7782 AGN and 3018 low-S/N SF galaxies. There are 2858 composite and 1362 star-forming galaxies, accounting for roughly 11 and 5 per cent of the total sample, respectively. As expected, most galaxies in the sample have specific star formation rates (SFR/M$_*$) less than $10^{-10.6}$ yr^{-1}, which are in most cases consistent with zero. We note that the distribution in specific star formation rates for the subclasses of C and SF galaxies shows a peak at $10^{-10.0}$ yr^{-1}.

Fig. 1 shows the distributions of several observational quantities of interest to us for this sample: the r-band absolute magnitude M_r, the $g - r$ colour, the logarithm of the velocity dispersion (in km s^{-1}) and the Mg$_2$ index strength. The magnitude M_r and the colour $g - r$ represent rest-frame quantities. They are corrected for evolution following the prescription of Bernardi et al. (2005), as described in Section 3.1.1. Also, the Mg$_2$ index strength is corrected to $z = 0$ assuming passive evolution, as described in Section 3.2. In each row, the solid histogram represents the distribution for each of the above subclasses (whose fractional contribution to the total sample is given in the leftmost panel), while the distribution for the sample as a whole is represented by the shaded grey histogram. The distributions for the unclassifiable, AGN and low-S/N SF galaxies agree well with the distributions for the sample as a whole. In contrast, C and especially SF galaxies tend to concentrate in the low-luminosity, blue, low velocity dispersion and low-Mg$_2$ tails of the distributions.

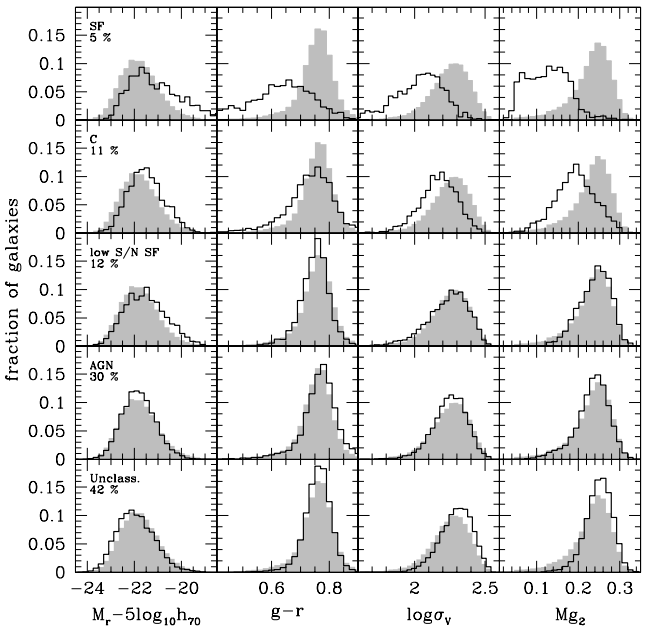

Figure 1. Distributions of the r-band absolute magnitude, $g - r$ colour (k-corrected to $z = 0$ and corrected for evolution following Bernardi et al. 2005), logarithm of velocity dispersion (in km s^{-1}) and Mg$_2$ index strength (in mag) for a sample of 26 003 early-type (high-concentration) SDSS DR2 galaxies with median S/N per pixel greater than 20 (grey histograms, repeated in all rows). From top to bottom, solid histograms in each row show the distributions for subsamples of galaxies classified by Brinchmann et al. (2004) according to their emission-line properties as star forming ('SF'), composite ('C'), low signal-to-noise ratio star forming ('low-S/N SF'), AGN ('AGN') and unclassifiable ('Unclass.', these are mainly galaxies with no emission lines). The fractional contributions by the different classes to the total sample of 26 003 early-type galaxies are indicated in the leftmost panels. All histograms are normalized to unit area.

The stellar metallicities, ages and stellar masses derived in Paper I for the galaxies in the sample are shown in Fig. 2 (shaded grey histograms). The distribution in metallicity extends from 0.4 to 2 Z$_\odot$ with a peak around $Z = 1.6$ Z$_\odot$. The distribution in r-band light-weighted age extends from 2.5 to 12 Gyr with a peak around $t_r = 9$ Gyr. The distribution in stellar mass extends from 10^{10} to 10^{12} M$_\odot$ with a peak around $M_* = 10^{11}$ M$_\odot$. The right-hand panels of Fig. 2 show the distributions of the associated errors, computed as one half the 68 per cent confidence ranges in the estimates of $\log(Z/Z_\odot)$, $\log(t_r/\mathrm{yr})$ and $\log(M_*/M_\odot)$. The typical uncertainty in both metallicity and age estimates is about ± 0.1 dex, while stellar mass is constrained to better than ± 0.1 dex for the majority of the galaxies in the sample. The same is true when considering Unclass., AGN and low-S/N SF galaxies only (solid histograms). The distributions for SF (dotted line) and C (dashed line) galaxies extend to lower stellar metallicities, ages and stellar masses than the bulk of the sample, with slightly higher errors in all three parameters.

In addition to the effects of age, metallicity and stellar mass, we are also interested in the influence of the α/Fe ratio on the observed properties of early-type galaxies. This ratio can be empirically quantified by the relative strengths of Mg- and Fe-based absorption-line indices (Thomas, Maraston & Bender 2003). We use here Mgb/$\langle$Fe$\rangle$, where $\langle$Fe$\rangle$ is the average of the Fe5270 and Fe5335 index strengths. In what follows, we compare the observed Mgb/$\langle$Fe$\rangle$ ratio of a galaxy to that of the model that best reproduces the five spectral features mentioned above. Since the models have

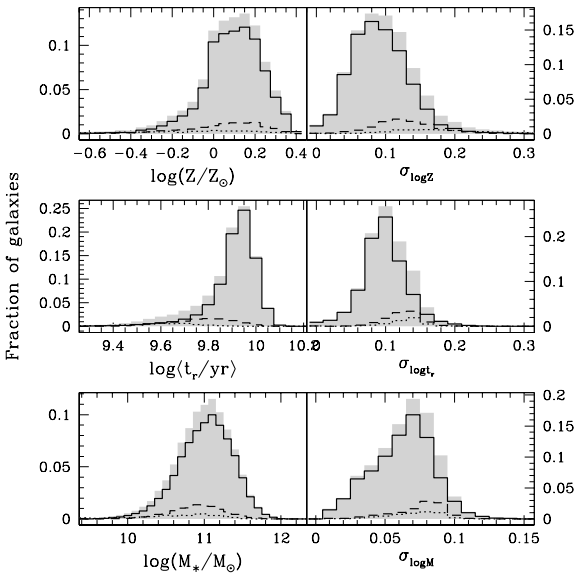

Figure 2. Left-hand panels: distributions of the median-likelihood estimates of stellar metallicity (top), r-band light-weighted age (middle) and stellar mass (bottom) for the same sample of early-type galaxies as in Fig. 1. The dotted histogram shows the distribution for SF galaxies, the dashed histogram for C galaxies and the solid histogram for the rest of the sample (Unclass., AGN and low-S/N SF). Right-hand panels: distributions of the associated errors, computed as one half the 68 per cent confidence ranges in the estimates of $\log(Z/Z_\odot)$, $\log(t_r/\mathrm{yr})$ and $\log(M_*/M_\odot)$.

scaled-solar abundance ratios, any discrepancy $\Delta(\mathrm{Mgb}/\langle\mathrm{Fe}\rangle)$ between observed and model index strengths can then be interpreted as a departure of the α-elements-to-iron abundance ratio from solar in the observed galaxy.

Working with the difference in index ratio rather than with the observed value of $\mathrm{Mgb}/\langle\mathrm{Fe}\rangle$ allows us to take into account the dependence of the index strength on age. It is also interesting to check whether the difference $\Delta(\mathrm{Mgb}/\langle\mathrm{Fe}\rangle)$ traces linearly the true α/Fe abundance ratio over the whole parameter space covered by our galaxies. It is not possible to check this self-consistently on our sample with our own models, since they do not include variations in element abundance ratios. For this test, we used simple stellar population (SSP) models with variable element abundance ratios from Thomas et al. (2003). We have considered SSPs with different α/Fe abundance ratios ([α/Fe] $= -0.2$, 0, 0.2, 0.4, 0.6), with age varying from 1 to 13 Gyr and metallicity varying from $\log(Z/Z_\odot) = -0.6$ to 0.5. For each model, we calculate the difference in $\mathrm{Mgb}/\langle\mathrm{Fe}\rangle$ with respect to the corresponding scaled-solar model at the same age and metallicity. We have looked at the relation between $\Delta(\mathrm{Mgb}/\langle\mathrm{Fe}\rangle)$ and the abundance ratio [α/Fe] at fixed metallicity. We do not find significant differences in the slope and zero-point of the linear relations, averaged over age, for different metallicities. Only at $\log(Z/Z_\odot) \sim -0.5$ is the relation somewhat flatter; we note that this is not relevant for the galaxies in our sample, which predominantly have metallicities above $\log(Z/Z_\odot) = -0.2$ (see Fig. 2). The proportionality between $\Delta(\mathrm{Mgb}/\langle\mathrm{Fe}\rangle)$ and [α/Fe] is confirmed by plotting $\Delta(\mathrm{Mgb}/\langle\mathrm{Fe}\rangle)$ as a function of age and as a function of metallicity for SSPs with different α/Fe ratio. At fixed [α/Fe], the measured $\Delta(\mathrm{Mgb}/\langle\mathrm{Fe}\rangle)$ is constant over the age and metallicity ranges covered by our sample. These checks reassure us that the discrepancy $\Delta(\mathrm{Mgb}/\langle\mathrm{Fe}\rangle)$ between the observed and the best-fitting model index strengths has the same proportionality with [α/Fe] over the age and metallicity ranges covered by the sample.

3 PHYSICAL ORIGIN OF OBSERVED RELATIONS FOR EARLY-TYPE GALAXIES

We use here the sample of 26 003 early-type galaxies described above to investigate the physical origin of two fundamental relations obeyed by early-type galaxies: the CMR (Section 3.1) and the Mg_2–σ_V relation (Section 3.2). We address the environmental dependence of these relations and of galaxy physical parameters in Section 3.3. We then explore in more detail how physical parameters are related to the depth of a galaxy's potential well (Section 3.4).

3.1 The colour–magnitude relation

The optical colours of early-type galaxies are strongly correlated with absolute magnitude, in the sense that bright galaxies tend to be redder than faint galaxies (e.g. Baum 1959; de Vaucouleurs 1961; Faber 1973; Visvanathan & Sandage 1977; Bower, Lucey & Ellis 1992). As mentioned in Section 1, the physical origin of this correlation is still a matter of controversy, mainly because of the lack of large samples of galaxies with accurate age and metallicity estimates.

3.1.1 Observed CMR

We consider here the CMR defined by the rest-frame $g - r$ colour and the absolute r-band magnitude M_r. We compute these quantities using the SDSS 'model' magnitudes, which are obtained from fits of the r-band surface brightness profile of each galaxy with either a de Vaucouleurs law or an exponential law (the best-fitting profile is also adopted in the other photometric bands). We k-correct the observed $g - r$ colour and the M_r absolute magnitude to $z = 0$ using the model in the spectral library of Section 2 that best reproduces the spectral absorption features of the galaxy, reddened to reproduce the observed colours at the redshift of the galaxy (this reddening correction is typically small; see below). We also correct colours and magnitudes for evolution, adopting the correction estimated by Bernardi et al. (2005) from a sample of 39 320 SDSS early-type galaxies, i.e. we make the magnitudes fainter by $0.85z$ and the colours redder by $0.3z$. From now on, we denote by M_r and $g - r$ the $k + e$-corrected (but not dereddened) quantities.

Fig. 3 shows the $g - r, M_r$ CMR defined in this way by early-type galaxies in the sample described in Section 2. We have arranged galaxies in bins of absolute magnitude and colour (0.15 and 0.01 width, respectively). The grey-scale indicates, for each magnitude bin, the relative distribution of galaxies in the different colour bins (we do not show bins containing less than 2 per cent of the total number of galaxies at a given magnitude). The straight line in Fig. 3 shows a ROBUST fit of these data, obtained by minimizing the absolute deviation in colour as a function of magnitude. We note that this lies slightly to the blue of the ridge line of the relation, reflecting the skewed colour distributions of Fig. 1. The robust fit has a slope[3] of -0.024 ± 0.002. This slope is consistent with that of -0.024 obtained previously by Bernardi et al. (2005).[4] The dashed lines in Fig. 3 show the mean positive and negative absolute deviations in colour (± 0.050) relative to this fit.

[3]The errors on the slopes of the fitted relations quoted throughout the paper have been estimated using a 'JACKKNIFE' method. The parameters of the fitted relations are summarized in Table 1.

[4]We estimated this slope as $\xi_\mathrm{CM}\,\sigma_\mathrm{CC}/\sigma_\mathrm{MM}$, using the values reported in tables 1 and 2 of Bernardi et al. (2005, see their appendix B1).

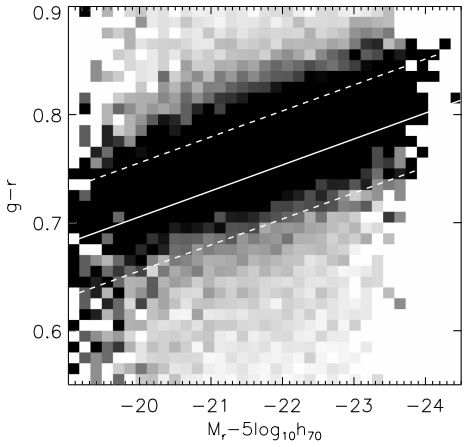

Figure 3. Relation between ($k + e$-corrected) $g - r$ colour and r-band absolute magnitude for the same sample of early-type galaxies as in Fig. 1. The grey-scale indicates, for each magnitude bin, the relative distribution of galaxies in the different colour bins (normalized along the colour axis). The solid line represents the relation between $g - r$ and M_r, fitted as described in the text. The dashed lines show the vertical scatter about the relation.

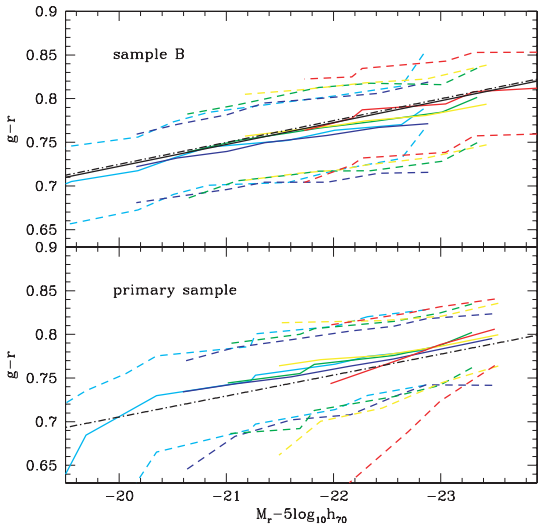

Figure 4. CMR for the same sample of early-type galaxies as in Fig. 1 (lower panel) and for a sample obtained using the same selection criteria as in Bernardi et al. (2005) (upper panel). The colours and luminosities of the galaxies in both samples are corrected for evolution following Bernardi et al. (2005; i.e. making $g - r$ redder by $0.3z$ and M_r fainter by $0.85z$). Different colours refer to different redshift intervals, $0.02 < z < 0.07$ (cyan), $0.07 < z < 0.09$ (blue), $0.09 < z < 0.12$ (green), $0.12 < z < 0.15$ (yellow), $0.15 < z < 0.2$ (red). For each redshift bin, solid and dashed lines give the median and the 68 per cent range in colour as a function of luminosity. Black dot–dashed lines show robust fits to the relations for the two samples (including galaxies at all redshifts), while the black solid line in the upper panel is the corresponding relation fitted by Bernardi et al. (2005) with a maximum-likelihood technique (see their fig. 2).

To better understand the influence of our galaxy selection criteria on our results, we constructed a second sample (we call this 'sample B') following the prescription by Bernardi et al. We first select all objects classified as galaxies, with measured velocity dispersions and with Petrosian r-band magnitudes (corrected for galactic reddening) between 14.5 and 17.75 in the SDSS DR2. We then define as early type those galaxies with fracDev_r > 0.8 and eclass < 0. We select in this way 59 907 early-type galaxies, for which we have $g - r$ colours and M_r absolute magnitudes.[5]

In Fig. 4, we compare the CMRs obtained from our primary sample and from sample B in different redshift bins (by analogy with fig. 2 of Bernardi et al. 2005). The black dot–dashed lines in Fig. 4 show robust fits to the relations for the two samples. The slope for sample B (-0.028 ± 0.001, upper panel) is in good agreement with that obtained by Bernardi et al. (2005; black solid line) and with that derived for our primary sample (-0.024 ± 0.002, lower panel). The colour–magnitude distributions of the galaxies in different redshift bins in sample B (upper panel) also agree reasonably well with those in fig. 2 of Bernardi et al. (2005). Thus, our results agree with those of Bernardi et al. (2005) under similar assumptions.

We note that our primary sample differs from sample B mainly through the inclusion of blue galaxies at intermediate-to-low luminosities. These are predominantly galaxies in the SF and C classes, which are likely to be bulge-dominated spiral galaxies with detectable emission lines (eclass > 0, which excludes them from sample B). The contamination of our primary sample by these galaxies also results from the fact that we do not make any distinction on the basis of galaxy environment. While the slope of the CMR in low-density environments is not significantly different from that found for cluster early-type galaxies, the scatter about the relation appears to increase from high- to low-density environments (Larson, Tinsley & Caldwell 1980; Hogg et al. 2004). Also, at the median redshift $z \sim 0.1$ of our sample, Pimbblet et al. (2002) find that, at fixed luminosity, early-type galaxies tend to have bluer colours in the outskirts than in the centres of galaxy clusters (see also Abraham et al. 1996). They interpret this as a difference in age of the galaxies in different environments.

As in other work on early-type galaxies (e.g. Bernardi et al. 2005), we do not include any correction for dust attenuation in the CMR presented here. We can estimate the influence of dust on the CMR, using the model spectral fits described in Section 2. The g- and r-band dust attenuation can be estimated from the difference between the emission-line corrected $r - i$ 'fibre'[6] colour of the galaxy and the $r - i$ colour of the redshifted, dust-free model, assuming a single power-law attenuation curve (see also Paper I). To quantify the effect of dust attenuation on the CMR, we show in Fig. 5 the average attenuation vectors (red arrows) for galaxies falling into different bins of $g - r$ and M_r (dashed boxes). As expected, the average attenuation is reduced if C and SF galaxies are excluded (blue arrows). In both cases, attenuation by dust becomes more important at lower luminosities. Correcting for dust attenuation would thus steepen the relation. When dereddening the colours and magnitudes of the galaxies in the sample according to the average attenuation vectors shown in Fig. 5, we derive a slope of -0.035 ± 0.002. Table 1 summarizes the parameters of the fits to the (k-corrected) CMR, with and without evolution and dust corrections.

3.1.2 *Physical origin of the CMR*

Fig. 6 shows how metallicity, age, α/Fe ratio and stellar mass change along the CMR. We have binned the $g - r, M_r$ plane in the same

[5]Note that the sample used by Bernardi et al. (2005) is slightly smaller than the SDSS DR2. Note also that sample B is larger than our primary sample, mainly because of our cut in the S/N ratio.

[6]fibre magnitudes are obtained from the flux measured within an aperture of radius 1.5 arcsec, i.e. equal to the fibre radius.

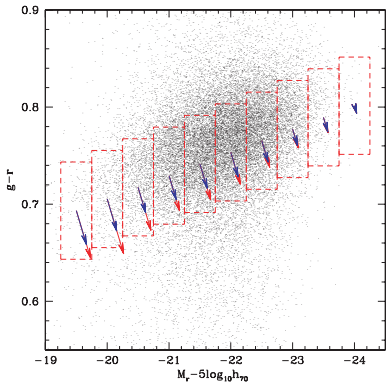

Figure 5. Relation between (k + e-corrected) $g - r$ colour and r-band absolute magnitude for the same sample of early-type galaxies as in Fig. 1. The red arrows indicate the average correction for dust attenuation on the colour and absolute magnitude of the galaxies falling into different $g - r$, M_r bins (indicated by the dashed boxes) along the fitted relation. The blue arrows indicate the average dust correction when galaxies in the star-forming and composite classes are excluded.

Table 1. Parameters of the relations fitted by minimizing the absolute vertical deviations. Sample A refers to our primary sample, while sample B is obtained by selecting galaxies according to Bernardi et al. (2005) criteria.

Sample	Slope	Intercept	Scatter
	Colour–magnitude relation		
Sample A[a]	-0.015 ± 0.001	0.40	0.051
Sample B[a]	-0.014 ± 0.002	0.41	0.043
Sample A[b]	-0.024 ± 0.002	0.22	0.050
Sample B[b]	-0.028 ± 0.001	0.14	0.043
Sample A[c]	-0.025 ± 0.001	0.14	0.051
Sample B[c]	-0.015 ± 0.002	0.37	0.043
Sample A[d]	-0.035 ± 0.002	-0.05	0.050
Sample B[d]	-0.029 ± 0.002	0.09	0.044
	Mg_2–σ_V relation		
Sample A[e]	0.23 ± 0.01	-0.29	0.024
Sample B[e]	0.17 ± 0.003	-0.15	0.023
Sample A[f]	0.25 ± 0.01	-0.31	0.024
Sample B[f]	0.19 ± 0.00	-0.18	0.023

[a] k-corrected colour and magnitude.
[b] $k + e$-corrected colour and magnitude (the evolution correction is the one provided by Bernardi et al. 2005).
[c] k-corrected colour and magnitude dereddened applying the average dust corrections of Fig. 5.
[d] Fully corrected colour and magnitude.
[e] Mg_2 index strength corrected for velocity dispersion.
[f] Mg_2 index strength corrected for velocity dispersion and evolution.

way as in Fig. 3, the brightness of each $g - r$ bin at a given M_r being proportional to the number of galaxies falling into this bin (see Section 3.1.1). In each panel, the colour code reflects the average properties of the galaxies falling into each colour–magnitude bin, as indicated. Panels (a)–(c) show how (the median-likelihood estimates of) age, metallicity and stellar mass are distributed along the CMR. Panel (d) shows the distribution of the offset $\Delta(\mathrm{Mgb}/\langle\mathrm{Fe}\rangle)$ between observed and predicted Mgb/⟨Fe⟩ index strengths, which traces the α-elements-to-iron abundance ratio (Section 2).

The most remarkable result from Fig. 6 is that the CMR is primarily a sequence in the stellar mass of early-type galaxies (panel c; note that the gradient in stellar mass is not exactly parallel to the magnitude axis, reflecting a non-constant mass-to-light ratio in the optical bands). Another striking result is that the average metallicity increases from $\sim$0.8 to $\sim 1.6\,Z_\odot$ from the faintest to the brightest galaxies along the relation, the average light-weighted age increasing by less than 3 Gyr (from 6.5 and 9.0 Gyr) over the same interval of 5 mag in M_r (panels a and b). The marked increase in metallicity is accompanied by an increase in the α-elements-to-iron abundance ratio (panel d). This is consistent with the finding that giant elliptical galaxies have higher [Mg/Fe] than faint elliptical galaxies (e.g., Worthey et al. 1992; Trager et al. 2000a; Kuntschner et al. 2001; Thomas et al. 2004). The gradients in both metallicity and age are not exactly parallel to the relation, but at fixed magnitude, bluer galaxies are more metal poor and younger than redder galaxies. Thus, both metallicity and age contribute to the scatter about the relation.

It is of interest to compare the relative contributions by age and metallicity to the scatter about the CMR. We note that we expect dust attenuation and changes in the [α/Fe] ratio to contribute negligibly to the scatter, since the scatter in $g - r$ colour of dust-free, [α/Fe] = 0 models with the ages and metallicities of the galaxies in our sample (± 0.041)[7] is very similar to the observed scatter (± 0.050). For comparison, the scatter in $g - r$ colour of models with the metallicities of the galaxies in our sample but with a fixed imposed (average) age at fixed M_r is only ± 0.022, while that of models with the ages of the galaxies in our sample but with a fixed imposed (average) metallicity at fixed M_r is ± 0.028. This indicates that age and metallicity contribute a similar amount to the scatter in the CMR for early-type galaxies.

Fig. 7 better quantifies the intrinsic scatter in the two physical parameters and how much it determines the scatter in colour as a function of stellar mass. The left-hand panels show the distribution in light-weighted age (or metallicity) as a function of $g - r$ colour in six bins of stellar mass (the median and the 16–84 interpercentile range are given by the red points and associated error bars). The right-hand panels show the marginalized distribution in age (metallicity) compared with a Gaussian of width equal to the average error in age (metallicity) for the galaxies in each stellar mass bin (dotted curve). From the left-hand plot, we can see that at masses above $10^{11}\,M_\odot$ the scatter in light-weighted age can be entirely accounted for by the measurement errors, which are on average less than 0.1 dex. We can thus say that all massive ellipticals of given mass have the same mean age (within the errors). At lower masses the scatter in light-weighted age becomes larger than the typical error, and the distribution is skewed towards younger ages. At fixed mass, there is a correlation between age and colour, which saturates for the reddest galaxies. We also detect a small intrinsic scatter in the mass–metallicity relation in all mass bins (right-hand plot), which contributes to the scatter in the CMR at fixed mass, even at the high-mass end.

It is important to check that aperture effects do not introduce any spurious trend in Fig. 6. This could arise because colour, luminosity and stellar mass pertain to the galaxy as a whole, while age, metallicity and $\Delta(\mathrm{Mgb}/\langle\mathrm{Fe}\rangle)$ are measured within a fixed fibre aperture of radius 1.5 arcsec, which samples different fractions of the total light in galaxies with different apparent sizes. In Section 3.4 of Paper I, we already showed that aperture effects are not expected to affect

[7] This is estimated by adopting, for each galaxy in the sample, the median of the likelihood distribution in $g - r$ obtained by weighting each model in the library of Section 2 by $\chi^2 = [(\log Z_{\rm mod} - \log Z)/\sigma_{\log Z}]^2 + [(\log t_{\rm mod} - \log t_r)/\sigma_{\log t_r}]^2$.

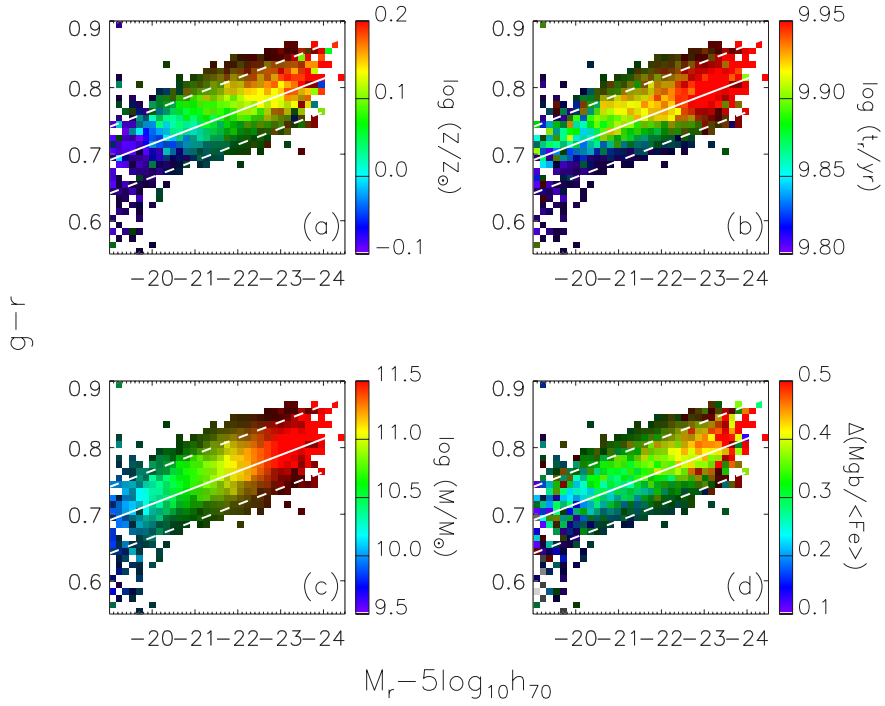

Figure 6. Relation between ($k + e$-corrected) $g - r$ colour and M_r absolute magnitude for the same sample of early-type galaxies as in Fig. 1. The CMR has been binned and colour coded to reflect the average stellar metallicity (panel a), r-band light-weighted age (panel b), stellar mass (panel c) and the α/Fe-indicator Δ(Mgb/$\langle$Fe$\rangle$) (panel d) of the galaxies falling into each bin. The shading indicates the fraction of galaxies populating each colour bin at fixed magnitude, according to the map of Fig. 3.

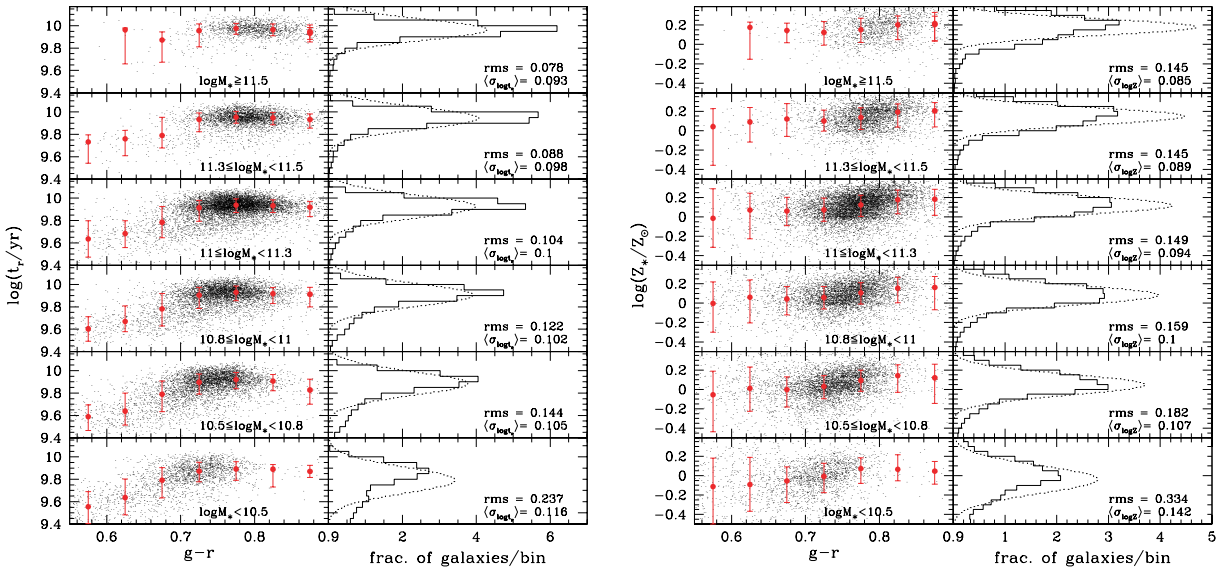

Figure 7. Left-hand panels: distribution in light-weighted age (left-hand plot) and stellar metallicity (right-hand plot) as a function of $g - r$ colour for different bins of stellar mass. The red dots are the median age (metallicity) at fixed colour, while the error bars give the 68 per cent percentile range in the age (metallicity) distribution. Right-hand panels: histogram of light-weighted age (metallicity) compared to a Gaussian (dotted curve) of width equal to the average error on age (metallicity) in each stellar mass bin. In each panel, the rms scatter and the average error in age (metallicity) are also given.

significantly the ages and metallicities derived for the galaxies in our sample. To probe the influence of aperture effects on the results of Fig. 6, we have arranged galaxies in several bins of apparent size $r_{50,r}$, defined as the r-band Petrosian half-light radius. Galaxies with $1.5 \lesssim r_{50,r} \lesssim 2.4$ arcsec are found out to redshift 0.2. We plotted the equivalent of Fig. 6 for each bin of $r_{50,r}$ within this range. In all cases, we found the same increase in metallicity, Δ(Mgb/$\langle$Fe$\rangle$) and age along the relation as in Fig. 6, although the trends were noisier because of the smaller numbers of galaxies in individual $r_{50,r}$ bins. In our sample, galaxies along the CMR have a roughly constant apparent size $r_{50,r} \sim 2.3$ arcsec at all magnitudes fainter than $M_r = -23.5$ (corresponding roughly to stellar masses less

than $10^{11.5}\,M_\odot$). The brightest galaxies tend to have larger apparent sizes, but stellar metallicity, age and $\Delta(\mathrm{Mgb}/\langle\mathrm{Fe}\rangle)$ do not show any significant trend with apparent size. Thus, we are confident that aperture effects are not responsible for the trends seen in Fig. 6.

For completeness, we repeated the analysis of Fig. 6 using sample B in place of our primary sample (Section 3.1.1). We found no significant difference in this case with respect to the results described above. We also repeated the analysis using our primary sample, but correcting the observed CMR for the effects of dust attenuation (Section 3.1.1). Again, the main results in this case did not change. We further checked the influence of a possible contamination of the trends identified in Fig. 6 by late-type galaxies, in particular, with regard to the variation in age along the relation. Excluding SF and C galaxies (which tend to have younger ages than the bulk of the sample) had no significant effect on the results. In fact, C galaxies alone display the same trends as found in Fig. 6 for the sample as a whole. The average metallicity of SF galaxies also increases with luminosity along the CMR, although these tend to have light-weighted ages clustered around a mean value $\log(t_r/\mathrm{yr}) = 9.6$ almost independent of luminosity. We note that SF galaxies represent only about 5 per cent of our primary sample, and they occupy $g-r$, M_r bins where the fraction of galaxies at a given magnitude is less than 2 per cent of the total sample (not displayed in Fig. 6).

In summary, we have shown that the CMR is primarily a sequence in galaxy stellar mass. Both the chemical composition (i.e. the total metallicity and the α-elements-to-iron abundance ratio) and the age of elliptical galaxies depend mainly on stellar mass, increasing along the relation. At the high-mass end of the relation, the age spread is negligible and consistent with the errors. In this regime, the scatter in the CMR is determined by the small scatter in the mass–metallicity relation. At lower masses, the distribution in age becomes broader, with a spread towards younger ages, which correlates with colour and is thus the main contributor to the scatter about the CMR at the low-luminosity end.

3.2 The $\mathrm{Mg_2}$–σ_V relation

In this section, we focus on another observational relationship between the stellar populations and the structural properties of early-type galaxies: the relation between $\mathrm{Mg_2}$ index strength and galaxy velocity dispersion σ_V (Bender et al. 1993). The difficulty in interpreting this relation comes from the complex translation of $\mathrm{Mg_2}$ index strength and σ_V into physical parameters.

The $\mathrm{Mg_2}$ index strengths considered here are corrected for broadening due to velocity dispersion. They are normalized to a fixed velocity dispersion of $\sigma_\mathrm{V} = 200\,\mathrm{km\,s^{-1}}$, corresponding roughly to the average velocity dispersion of galaxies in our sample. The normalization is achieved by using the Bruzual & Charlot (2003) models to compute the difference in $\mathrm{Mg_2}$ index strength between the observed and reference velocity dispersion at the metallicity of each galaxy.[8] For a consistent comparison with the CMR and with the evolution-corrected light-weighted ages, we also correct the $\mathrm{Mg_2}$ index strengths so that they are relative to the present rather than to the redshift of observation, assuming passive evolution. The corrections are obtained by fitting simple linear relations between $\mathrm{Mg_2}$ index strength and time for SSPs of different metallicities and velocity dispersions. The $\mathrm{Mg_2}$ value measured for each galaxy is then corrected by adding the expected change in index strength over a time interval equal to the look-back time at the redshift of the galaxy.[9]

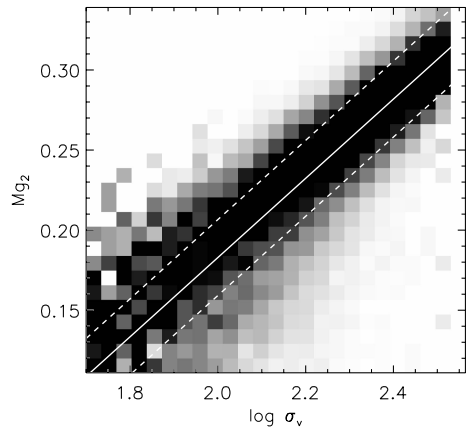

Figure 8. Relation between $\mathrm{Mg_2}$ index strength (mag) and velocity dispersion $\log\sigma_\mathrm{V}(\mathrm{km\,s^{-1}})$ for the same sample of early-type galaxies as in Fig. 1. As in Fig. 3, the grey-scale indicates, for each velocity dispersion bin, the relative distribution of galaxies in the different $\mathrm{Mg_2}$ bins.

Fig. 8 shows the $\mathrm{Mg_2}$–σ_V relation defined by the early-type galaxies in our primary sample. We have arranged galaxies in narrow bins of $\mathrm{Mg_2}$ and $\log\sigma_\mathrm{V}$ (of widths 0.01 and 0.036, respectively). By analogy with Fig. 3, the grey-scale in Fig. 8 indicates, for each $\log\sigma_\mathrm{V}$ bin, the relative distribution of galaxies in the different $\mathrm{Mg_2}$ bins (we do not show bins containing less than 2 per cent of the total number of galaxies at given velocity dispersion). The solid straight line shows the result of a robust linear fit obtained by minimizing the absolute deviation in $\mathrm{Mg_2}$ strength as a function of $\log\sigma_\mathrm{V}$. This has a slope of 0.25 ± 0.01, i.e. very close to that found by Bernardi et al. (2003d) for a sample of co-added, high-quality spectra of SDSS early-type galaxies (see also Guzman et al. 1992; Colless et al. 1999). The dashed lines in Fig. 8 are the mean positive and negative absolute deviations in $\mathrm{Mg_2}$ strength (± 0.024 mag) relative to this fit (also in agreement with previous work). These results are summarized in Table 1. We also indicate in the table the slightly lower slope of the $\mathrm{Mg_2}$–σ_V relation obtained for sample B (0.19 ± 0.002). This is because sample B includes fewer (emission-line) galaxies with weak $\mathrm{Mg_2}$ absorption than our primary sample at low σ_V and more (low-S/N) galaxies with weak $\mathrm{Mg_2}$ absorption at large σ_V (Section 3.1.1).

The tightness of the $\mathrm{Mg_2}$–σ_V relation has been used in the past to argue that early-type galaxies have nearly coeval stellar populations, perhaps within $\sim$15 per cent, at given composition (e.g. Bender et al. 1993). However, as noted by Trager et al. (2000a), the small scatter about the relation could also conceal significant age spreads, if these are accompanied by metallicity spreads such that the $\mathrm{Mg_2}$ strength remains roughly constant at fixed velocity dispersion (see also Jørgensen 1999). Assuming a moderate anticorrelation between age and metallicity, Colless et al. (1999) find that the intrinsic scatter in the $\mathrm{Mg_2}$–σ_V relation translates into an upper limit of 40 (50) per cent on the age (metallicity) spread. Moreover, it has been pointed out that, at fixed σ_V, the distribution of $\mathrm{Mg_2}$ residuals relative to the mean $\mathrm{Mg_2}$–σ_V relation is not symmetric but skewed towards

[8]This correction varies from -0.002 to 0.004 over the range in velocity dispersion covered by the sample. The average absolute correction is only 0.8 per cent of the 5–95 per cent percentile range in $\mathrm{Mg_2}$ index strength.

[9]The fitted slopes, averaged over velocity dispersion, are $0.0056, 0.0044, 0.0064, 0.0077\,\mathrm{mag\,Gyr^{-1}}$ for $\log(Z/Z_\odot) = -0.7, -0.4, 0, 0.4$, respectively.

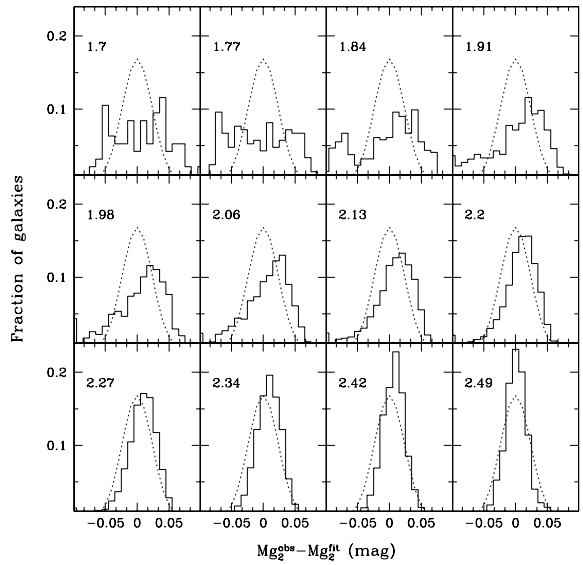

Figure 9. Distribution of residuals relative to the mean Mg_2–σ_V relation fitted in Fig. 8, for different values of $\log(\sigma_V/\mathrm{km\,s^{-1}})$ (indicated in each panel). The number of galaxies is normalized to the total in each bin of velocity dispersion. The dotted curve (repeated in each panel) is a Gaussian distribution of width equal to the average absolute deviation in the Mg_2–σ_V relation (see Table 1).

low Mg_2 values, and that this effect tends to increase at low velocity dispersion (Burstein et al. 1988; Bender et al. 1993; Jørgensen, Franx & Kjaergaard 1996; Trager et al. 2000a; Worthey & Collobert 2003). Our data confirm this finding. Fig. 9 shows the distribution of Mg_2 residuals at different velocity dispersions (increasing from the top left-hand to the bottom right-hand panels) for our primary sample. At large velocity dispersion, the distribution of residuals is symmetric and centred around zero, while at smaller velocity dispersions, a tail of negative residuals appears. This could result from either an age or a metallicity spread, or both. The observation that galaxies with negative residuals are often morphologically disturbed (presumably because of recent star formation) led to the idea that low Mg_2 values at fixed σ_V are associated with younger ages (Schweizer & Seitzer 1992).

The availability of independent constraints on the ages and metallicities of early-type galaxies in our sample allows us to re-examine the physical origin of the Mg_2–σ_V relation. Fig. 10 shows how metallicity, age, α/Fe ratio and stellar mass change along this relation. We have binned and colour coded the Mg_2, σ_V plane to reflect the average properties of the galaxies falling into each bin. As in Fig. 8, the brightness of each Mg_2 bin at a given σ_V is proportional to the number of galaxies falling into this bin. Panels (a)–(c) show how (the median-likelihood estimates of) age, metallicity and stellar mass are distributed along the Mg_2–σ_V relation. Panel (d) shows the distribution of the offset $\Delta(\mathrm{Mgb}/\langle\mathrm{Fe}\rangle)$ between observed and predicted Mgb/⟨Fe⟩ index strengths, which traces the α/Fe ratio (Section 2).

The most remarkable result from Fig. 10 is that, like the CMR, the Mg_2–σ_V relation for early-type galaxies appears to be primarily a sequence in stellar mass (panel c). In fact, stellar mass correlates tightly with velocity dispersion, which is a tracer of dynamical mass (e.g. Cappellari et al. 2006). Panel (a) further shows that stellar metallicity increases along the relation, from $\sim$0.8 to 1.6 $Z_\odot$ from low- to high-velocity dispersions. Galaxies with large σ_V are also older than those with low σ_V, though for $\log\sigma_V \lesssim 2.3$ age appears to correlate with Mg_2 index strength as well. Another striking result from Fig. 10 is the similarity between the metallicity and $\Delta(\mathrm{Mgb}/\langle\mathrm{Fe}\rangle)$ gradients along the Mg_2–σ_V relation (panels a and d). This shows that massive early-type galaxies with large velocity dispersions are both more metal rich and more abundant in α elements relative to iron than less massive galaxies.

As in the case of the CMR (Section 3.1.2), we have checked that the trends identified above are not caused by aperture effects. In particular, we find similar trends in stellar mass, metallicity, age and $\Delta(\mathrm{Mgb}/\langle\mathrm{Fe}\rangle)$ along the Mg_2–σ_V relation when considering galaxies in narrow ranges of $r_{50,r}$. Galaxies along the relation have roughly constant apparent size $r_{50,r} \sim 2.3$ arcsec, implying that the average fraction of total galaxy flux sampled by the fibre is almost constant.

As above for the CMR, we can quantify the relative contribution of metallicity and age to the scatter in the Mg_2–σ_V relation. We note that there must be another parameter, most likely the α-elements-to-iron abundance ratio, that is responsible for the scatter in the relation. In fact, the scatter in Mg_2 of $[\alpha/\mathrm{Fe}] = 0$ models with the ages and metallicities of the galaxies in our sample is only $\pm$0.0118, i.e. much smaller than the observed scatter (0.0237).[10] We obtain a similar scatter ($\pm$0.0116) in the Mg_2 index strength of models with the same metallicity as the galaxies in our sample but with a fixed imposed (average) age at fixed $\log\sigma_V$. On the other hand, the scatter in Mg_2 index strength of models with the ages of the galaxies in our sample but with a fixed imposed (average) metallicity at fixed $\log\sigma_V$ is only $\pm$ 0.007. This indicates that metallicity has a stronger influence than age on the scatter in the Mg_2–σ_V relation.

Fig. 11 is obtained in a similar way as Fig. 7. As in Fig. 7, the left-hand panels of Fig. 11 show that the scatter in light-weighted age of high-mass ellipticals ($M_* \geqslant 10^{11}\,M_\odot$) is negligible and consistent with the errors on the age estimates. Only at masses below $10^{11}\,M_\odot$ does a significant tail of younger ages appear. These young galaxies are responsible for the scatter in Mg_2 at fixed mass, but the relation between age and index strength saturates for $Mg_2 \gtrsim 0.25$. Also in agreement with Fig. 7, the right-hand plot shows that we detect (above the measurement error) a small scatter in metallicity at fixed mass in all mass bins. There is a correlation between metallicity and Mg_2 at fixed mass, in particular for galaxies with $Mg_2 \gtrsim 0.25$ (left-hand panels), where light-weighted age saturates to a constant mean value.

The Mg_2–σ_V relation is, therefore, primarily a sequence in galaxy stellar mass. It reflects the fact that early-type galaxies form a sequence of increasing total stellar metallicity and α-elements to iron abundance ratio from shallow to deep potential wells. Our results also confirm the trend of increasing age with increasing velocity dispersion (e.g. Caldwell, Rose & Concannon 2003; Nelan et al. 2005; Thomas et al. 2005). At high masses, the small scatter in the relation correlates with the scatter in stellar metallicity at fixed stellar mass, while light-weighted age is almost independent of index strength. At the low-mass end of the relation, the fraction of young ellipticals increases and variations in age between $\sim$4 and $\sim$8 Gyr correlate with index strength at fixed mass.

3.3 Environmental dependence

Several authors have addressed the dependence on environment of the properties of the stellar populations in early-type galaxies.

[10] For each galaxy in the sample, we adopt here the median of the likelihood distribution in Mg_2 obtained by weighting each model by $\chi^2 = [(\log Z_{\mathrm{mod}} - \log Z)/\sigma_{\log Z}]^2 + [(\log t_{\mathrm{mod}} - \log t_r)/\sigma_{\log t_r}]^2$.

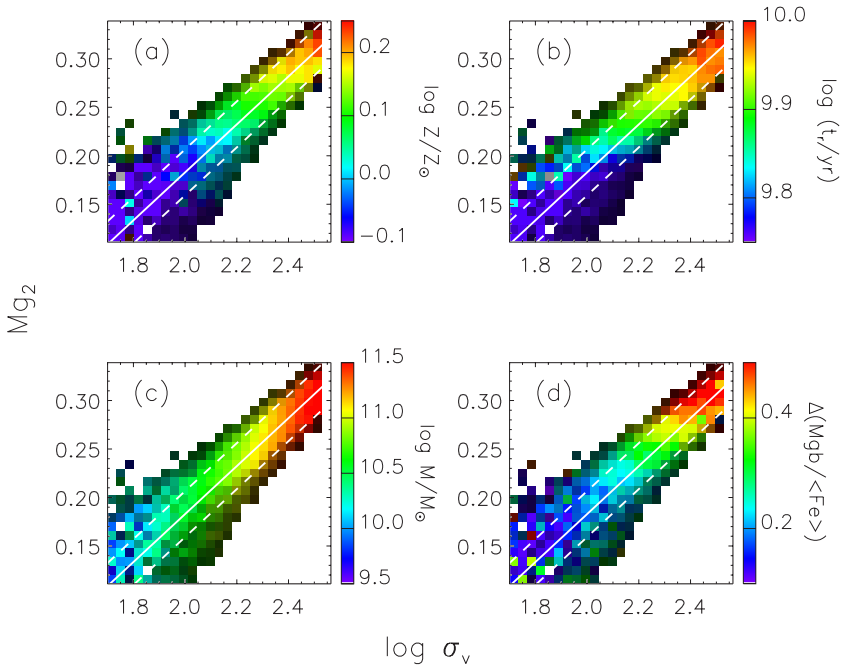

Figure 10. Relation between Mg_2 index strength (mag) and velocity dispersion (km s^{-1}) for the same sample of early-type galaxies as in Fig. 1. The relation has been binned and colour coded to reflect the average stellar metallicity (panel a), r-band light-weighted age (panel b), stellar mass (panel c) and α/Fe-estimator Δ (Mgb/⟨Fe⟩) (panel d) of the galaxies falling into each bin. The shading indicates the fraction of galaxies populating each Mg_2 bin a fixed $\log \sigma_V$, according to the map of Fig. 8.

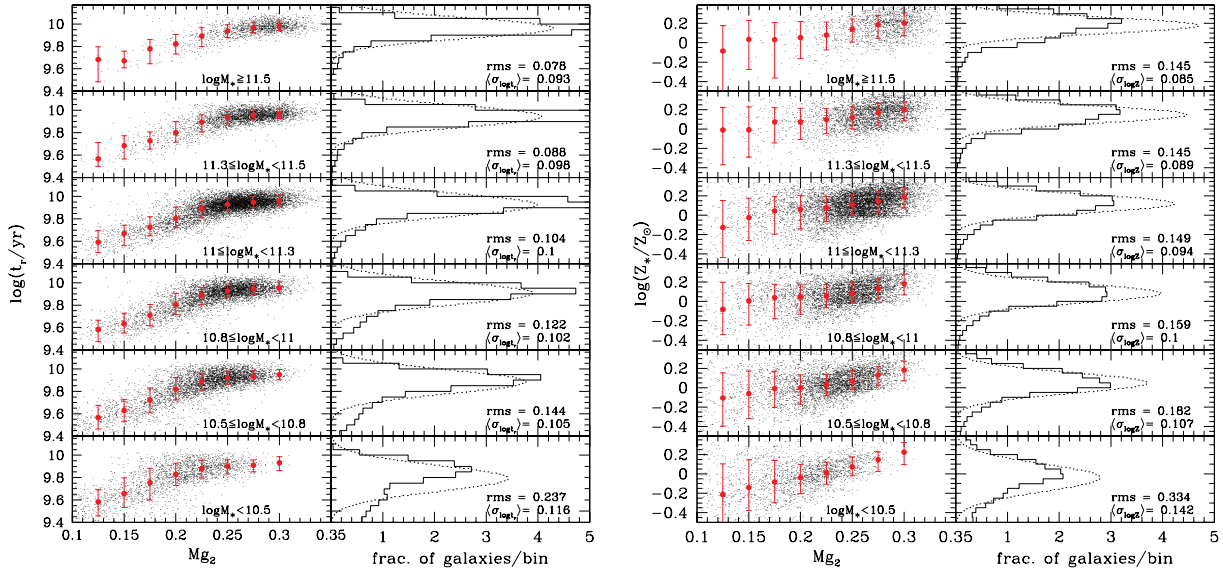

Figure 11. Left-hand panels: light-weighted age (left-hand plot) and stellar metallicity (right-hand plot) as a function of Mg_2 index strength (mag) in different bins of stellar mass. The red dots with error bars represent the median and the 68 per cent percentile range of the age (metallicity) distribution at given Mg_2 index strength. Right-hand panels: histogram of light-weighted age (metallicity) compared to a Gaussian (dotted curve) of width given by the average error in age (metallicity) for the galaxies falling into each stellar mass bin. The scatter and the average error in age (metallicity) are also indicated.

Studies of the CMR and the relations between absorption indices and velocity dispersion on relatively small samples of early-type galaxies in different environments have shown that galaxies in low-density environments tend to be younger and more metal rich than those in high-density environments (e.g. Kuntschner et al. 2002; Denicoló et al. 2005; Thomas et al. 2005). Bernardi et al. (1998), later confirmed by Bernardi et al. (2006) on a larger sample of SDSS early-type galaxies, found differences in the Mg_2–σ_V relation of galaxies in different environments, implying that galaxies in dense environments are at most 1-Gyr older than galaxies in low-density environments and that they have the same metallicity.

Kauffmann et al. (2004) provide estimates of environmental density for a sample of SDSS DR2 galaxies in the redshift range $0.03 < z < 0.1$ and with apparent r-band magnitude in the range $14.5 < r <$

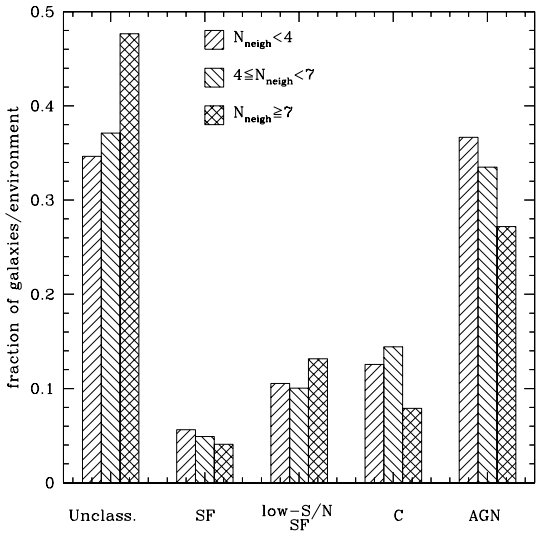

Figure 12. Fraction of unclassifiable ('Unclass.'), star-forming ('SF'), low-S/N star-forming ('low-S/N SF'), composite ('C') and AGN galaxies as a function of environment. Three different bins of environmental density are considered here, as given by $N_{\rm neigh}$ in the plot. Each histogram is normalized to the number of galaxies in the corresponding environmental bin. While the high-density environments are strongly dominated by galaxies without emission lines (unclassifiable), the fraction of star-forming, composite and AGN galaxies increases in lower density environments.

17.77, complete down to a stellar mass of $2 \times 10^9\,{\rm M}_\odot$. The density is expressed in terms of the number of spectroscopically observed neighbouring galaxies (down to a fixed absolute magnitude) within 2 Mpc of projected radius and ± 500 km s^{-1} in velocity difference from the target galaxy, corrected for galaxies missed due to fibre collisions ($N_{\rm neigh}$). We take advantage of these density estimates to address any environmental dependence of the physical properties of the stellar populations for the galaxy sample studied here. This can be achieved for only 1765 galaxies in our sample, for which an estimate of $N_{\rm neigh}$ is available. We consider three bins in environmental density, defined by $N_{\rm neigh} < 4, 4 \leqslant N_{\rm neigh} < 7$ and $N_{\rm neigh} \geqslant 7$, which contain, respectively, 693, 388 and 684 galaxies. As mentioned in Section 2, we can classify the galaxies in our sample on the basis of their emission-line properties. As expected, the sample is dominated by 'unclassifiable' galaxies (without emission lines), but there is also contamination by galaxies with a low level of star formation (SF and C galaxies). Fig. 12 illustrates the fraction of unclassifiable, SF, low-S/N SF, C and AGN galaxies as a function of environment. This plot quantifies the statement of Section 3.1.1 that the fraction of galaxies showing emission lines in our sample increases in lower density environments. This class of galaxies also contributes to increase the scatter blueward of the CMR.

In Fig. 13, we explore how the CMR (left-hand panels) and the $\rm Mg_2$–$\sigma_{\rm V}$ relation (right-hand panels) depend on environment. The relations found in the highest-density bin are compared to those defined in the lowest-density bin. The results of the linear fits (also for the intermediate bin of $N_{\rm neigh}$) are given in Table 2. Fig. 13 and Table 2 show that there is no systematic variation in the slope of the CMR as a function of environment, while the $\rm Mg_2$–$\sigma_{\rm V}$ relation appears to steepen at low densities because of a larger fraction of galaxies with low $\rm Mg_2$ index strength at low velocity dispersions (Columns 3 and 6). Between the two extreme density bins, there are differences of 0.006 ± 0.003 and 0.007 ± 0.003 in the zero-points of the CMR and the $\rm Mg_2$–$\sigma_{\rm V}$ relation, respectively (Columns 4 and 7). This is in agreement with the small shift of 0.007 ± 0.002 mag measured by Bernardi et al. (1998) in the $\rm Mg_2$–$\sigma_{\rm V}$ relation of a sample of 931 early-type galaxies in different environments. We also identify a systematic increase of the scatter about both relations from high- to low-density environments, in agreement with earlier findings, as mentioned above (e.g. Hogg et al. 2004).

It is of interest to understand how the change in the scatter along the two scaling relations reflects differences in the physical parameters of galaxies in different environments. We note that the distribution in stellar mass does not vary significantly[11] with environment, but that the median stellar mass of galaxies in the lowest-density bin is lower by about 0.05 dex than the median stellar mass in the highest-density bin (it increases from 8×10^{10} to $9 \times 10^{10}\,{\rm M}_\odot$). Since stellar metallicity, age and element abundance ratio all increase with stellar mass, any effect induced by changes in stellar mass must be removed when quantifying variations in these parameters with environment. To do this, we calculate the median stellar metallicity, light-weighted age and element abundance ratio as a function of stellar mass for the sample as a whole (see Fig. 17). For the 1765 galaxies with an estimate of environmental density, we then consider the offsets in $\log(Z/{\rm Z}_\odot), \log(t_r/{\rm yr}), \Delta({\rm Mgb}/\langle{\rm Fe}\rangle)$ from the median values of these parameters at fixed stellar mass in the whole sample. The distributions in $\Delta[\log Z]$ and $\Delta[\log t_r]$ are skewed towards negative values, independent of environment, and this effect is stronger at small masses. If galaxies at low densities are distributed preferentially to smaller masses than galaxies in dense environments, the distributions in $\Delta[\log Z]$ and $\Delta[\log t_r]$ will show a stronger tail towards negative values in the low-density bin. To separate this effect from an intrinsic dependence of metallicity and age on environment, we further distinguish between galaxies with stellar masses above and below $10^{11}\,{\rm M}_\odot$.

The result of this analysis is shown in Fig. 14 for the same three environmental bins as considered above. The distributions of the offsets in $\log(Z/{\rm Z}_\odot), \log(t_r/{\rm yr})$ and $\Delta({\rm Mgb}/\langle{\rm Fe}\rangle)$ for the two low-density bins ($N_{\rm neigh} < 4$ and $4 \leqslant N_{\rm neigh} < 7$, solid lines) are compared to the corresponding ones in the high-density bin ($N_{\rm neigh} \geqslant 7$, dotted line in each panel), for massive and low-mass galaxies separately (red and blue histograms, respectively). The comparison is also summarized in Table 3, where we give the difference of the average parameter offset between the highest- and the lowest-density bins, for galaxies with stellar mass above and below $10^{11}\,{\rm M}_\odot$ separately. There, we also indicate the probability for the two distributions to be drawn from the same parent distribution, according to a KS test. Element abundance ratio, as expressed by $\Delta({\rm Mgb}/\langle{\rm Fe}\rangle)$, does not show any significant variation with environment, either in the average value or in the scatter. In contrast, light-weighted age (independent of mass) and metallicity (for massive galaxies) show a small dependence on environment in the sense that there is a higher fraction of young, metal-poor galaxies in low-density environments. Massive early-type galaxies in dense environments tend to be $\sim$0.03 dex more metal rich than their field counterparts. Similarly, the light-weighted ages of galaxies in dense environments are $\sim$0.02-dex older than in the field. It is interesting to mention that we also find a systematic increase in the scatter of metallicity and age from dense to low-density environments. From the highest- to the lowest-density bins, the

[11] When comparing the stellar mass distribution of galaxies in the low-density bin with that of galaxies in the high-density bin, the probability obtained from a Kolmogorov–Smirnov (KS) test is not low enough to reject the hypothesis that the two distributions are drawn from the same parent distribution.

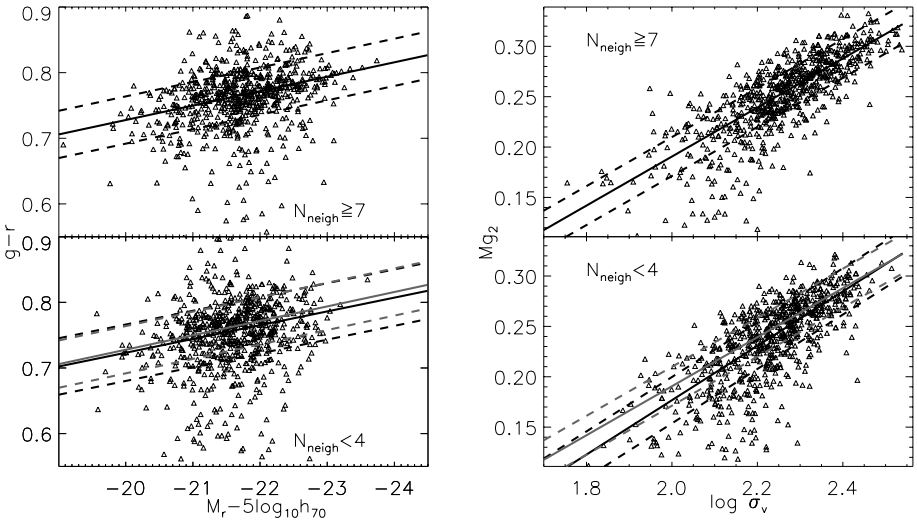

Figure 13. Colour–magnitude (left-hand plot) and Mg_2–σ_V relations (right-hand plot) as a function of environment. Galaxies are divided into two disjoint bins of environmental density (increasing from bottom to top as indicated by N_{neigh} in each panel). The linear relation fitted for each subsample and the scatter about it are shown in each panel by the black solid and dashed lines. The grey lines reproduce the relation fitted in the highest density bin.

Table 2. Parameters of the CMR (Columns 3, 4, 5) and Mg_2–σ_V relation (Columns 6, 7, 8) for a subsample of 1765 galaxies with environmental estimates. The relations are fitted separately for three different bins of environmental density (given by N_{neigh}, Column 1). The number of galaxies in each bin is given in Column 2. The intercepts are given at $M_r = -21.5$ and $\log \sigma_V = 2.25$, which correspond roughly to the average magnitude and velocity dispersion of this subsample of galaxies.

Environment	N_{gal}	Colour–magnitude			Mg_2–σ_V		
		Slope	Intercept	Scatter	Slope	Intercept	Scatter
(1)	(2)	(3)	(4)	(5)	(6)	(7)	(8)
$N_{neigh} < 4$	693	-0.021 ± 0.004	0.755 ± 0.002	0.043	0.27 ± 0.03	0.244 ± 0.002	0.023
$4 \leqslant N_{neigh} < 7$	388	-0.026 ± 0.006	0.757 ± 0.004	0.041	0.26 ± 0.01	0.242 ± 0.001	0.020
$N_{neigh} \geqslant 7$	684	-0.022 ± 0.003	0.761 ± 0.003	0.036	0.24 ± 0.02	0.251 ± 0.003	0.019

scatter in both metallicity and age increases by about 0.02 dex for massive galaxies (from 0.118 to 0.135 for $\log(Z/Z_\odot)$, from 0.083 to 0.103 for $\log(t_r/\mathrm{yr})$) and by about 0.01 dex for $M_* < 10^{11}\,M_\odot$ (from 0.16 to 0.17 for $\log(Z/Z_\odot)$ and from 0.12 to 0.136 for $\log(t_r/\mathrm{yr})$). Although very small, these trends hint at a possibly very relevant environmental dependence of metallicity and age. Future analysis of larger samples of galaxies (provided e.g. by the complete SDSS) with well-characterized environmental properties will allow us to draw firmer conclusions.

3.4 Correlations between physical parameters

So far, we have considered separately the constraints set by the colour–magnitude and the Mg_2–σ_V relations on the ages, chemical compositions and stellar masses of early-type galaxies in our sample. Here, we explore in more detail the potential correlations between these different physical parameters, the dynamical mass and the stellar surface mass density of galaxies.

We first turn our attention to the relation between age, luminosity, velocity dispersion and stellar mass inferred from the distribution in the full parameter space described by the colour–magnitude and the Mg_2–σ_V relations. Figs 6(b) and 10(b) taken together indicate that brighter galaxies or galaxies with large velocity dispersions are on average older than fainter or smaller velocity dispersion ones (consistent with the 'downsizing' scenario; Cowie et al. 1996; see also Section 4). In Fig. 15(a), we show the relation between M_r absolute magnitude, velocity dispersion σ_V and light-weighted age for the galaxies in our primary sample. At fixed luminosity, galaxies with large σ_V tend to be older than those with small σ_V (a result already pointed out by Forbes & Ponman 1999 and Bernardi et al. 2005). Conversely, at fixed velocity dispersion, luminous galaxies tend to be younger than faint galaxies. The dispersion in the M_r–σ_V relation and the dependence of luminosity on age at fixed σ_V cannot be accounted for entirely by the fact that the stellar mass-to-light ratio M_*/L_r of an evolving stellar population increases with light-weighted age. This is shown in Fig. 15(b), where we plot the relation between stellar mass and velocity dispersion for the same galaxies as in Fig. 15(a). The scatter of 0.252 dex about this relation is consistent with the scatter of 0.579 mag in the relation between M_r and σ_V. There appears to be a real dependence of age on stellar mass at fixed velocity dispersion, in the sense that galaxies with large stellar masses tend to be slightly younger than those with low stellar masses (Table 4 provides simple linear fits to the relations shown in Figs 15a and b).

The results of Fig. 15 motivate us to investigate more closely the relation between stellar mass and dynamical mass for early-type galaxies. We can estimate the dynamical mass (including stars and dark matter) within the optical radius of a galaxy from a combination of velocity dispersion and optical size (Cappellari et al. 2006). Here we use the radius containing 50 per cent of the Petrosian flux in the r band ($R_{50,r}$) rather than the effective de Vaucouleurs radius (r_{deV}) because we do not explicitly select early-type galaxies on the basis of the shape of their light profile. Thus, a de Vaucouleurs profile may not always be an optimal fit to the photometric data,

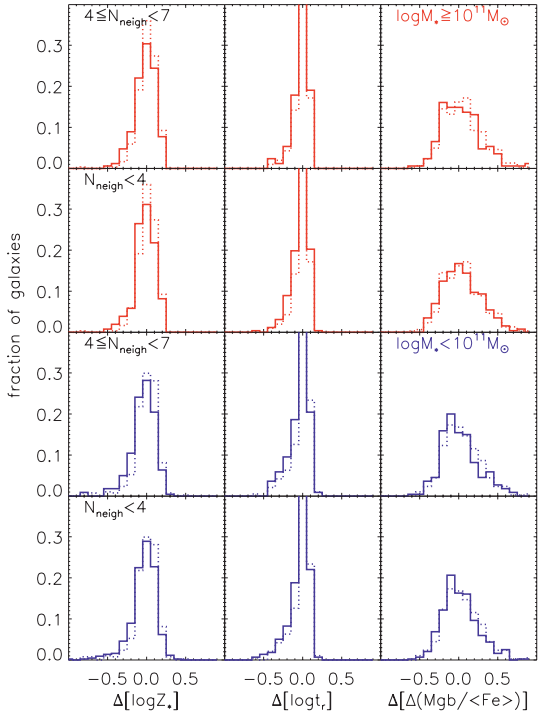

Figure 14. Stellar metallicity, age and element abundance ratio (expressed as $\Delta(\mathrm{Mgb}/\langle\mathrm{Fe}\rangle)$) as a function of environment for the subsample of 1765 galaxies with environmental estimates. We have estimated the offset in $\log(Z/Z_{\odot})$, $\log(t_r/\mathrm{yr})$ and $\Delta(\mathrm{Mgb}/\langle\mathrm{Fe}\rangle)$ from the median value at fixed stellar mass calculated for the sample as a whole. The distributions in the offsets are more skewed towards negative values at smaller masses. Thus, to further remove any effect induced by an environmental dependence of the mass, we analysed separately galaxies with masses above and below $10^{11}\,\mathrm{M}_{\odot}$ (shown in red and blue, respectively). For each stellar mass bin, the distributions in the offsets are shown for galaxies with different environmental density ($N_{\mathrm{neigh}} < 4$ in the lower panels and $4 \leqslant N_{\mathrm{neigh}} < 7$ in the upper panels, solid line). Each distribution is compared to that for galaxies with $N_{\mathrm{neigh}} \geqslant 7$, shown by the dotted line in each panel.

and the empirical half-light radius $R_{50,r}$ is more straightforward to interpret.[12] To estimate the dynamical mass within $R_{50,r}$, we must also account for the fact that the velocity dispersion of SDSS galaxies is measured within a fixed 1.5-arcsec fibre radius. Following Jørgensen (1999), we assume that the radial profile of the velocity dispersion has a slope −0.04. The velocity dispersion at the radius $R_{50,r}$ is then given by

$$\frac{\sigma_{\mathrm{V}}(r_{\mathrm{fibre}})}{\sigma_{\mathrm{V}}(R_{50,r})} = \left(\frac{r_{\mathrm{fibre}}}{R_{50,r}}\right)^{-0.04}, \quad (1)$$

and the dynamical mass within $R_{50,r}$ by

$$\frac{M_{\mathrm{dyn}}}{\mathrm{M}_{\odot}} = \xi \frac{\sigma_{\mathrm{V}}^2(R_{50,r})\, R_{50,r}}{G}. \quad (2)$$

In this expression, G is the gravitational constant, and ξ is a scaling factor given in Table 5, which depends on the shape of the velocity dispersion profile (this factor would be equal to 5 if we estimated the dynamical mass within the effective de Vaucouleurs radius; see Cappellari et al. 2006).

In Fig. 16, we compare the dynamical masses obtained in this way to the stellar masses derived in Paper I for the early-type galaxies in our primary sample.[13] We focus on the slope of the relation

[12]The de Vaucouleurs effective radii of the galaxies in our sample are on average ∼1.4 times larger than the Petrosian half-light radii. This arises presumably from the fact that the Petrosian flux represents typically 80 per cent of the total flux in the de Vaucouleurs model (Padmanabhan et al. 2004), but this could also result (at least for a class of objects) from forcing a de Vaucouleurs fit to a flatter galaxy light profile.

Table 3. Difference between the average parameter offset between the $N_{\mathrm{neigh}} < 4$ and $N_{\mathrm{neigh}} \geqslant 7$ environmental bins, distinguishing between galaxies with stellar masses above and below $10^{11}\,\mathrm{M}_{\odot}$. For each parameter, the second row gives the probability from a KS test that the two distributions are consistent with being drawn from the same parent distribution (we consider differences to be statistically significant only if the KS probability is below 1 per cent).

	$M_* \geqslant 10^{11}\,\mathrm{M}_{\odot}$	$M_* < 10^{11}\,\mathrm{M}_{\odot}$
$\Delta[\log Z]$	0.032 ± 0.006	0.029 ± 0.006
	0.0030	0.0217
$\Delta[\log t_r]$	0.019 ± 0.005	0.023 ± 0.006
	0.0053	0.0017
$\Delta[\Delta(\mathrm{Mgb}/\langle\mathrm{Fe}\rangle)]$	0.008 ± 0.009	0.024 ± 0.009
	0.5321	0.1499

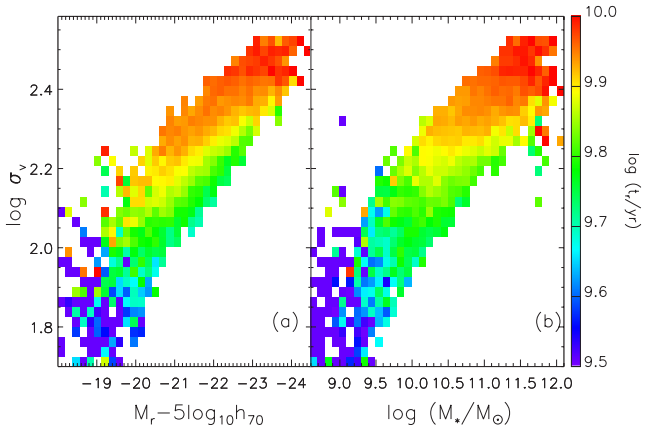

Figure 15. Relation between velocity dispersion and r-band absolute magnitude (panel a), colour coded to reflect the average light-weighted age of the galaxies falling into each $\log\sigma_{\mathrm{V}}$–M_r bin. For M_r brighter than −20, lines of constant age are approximately parallel to the relation. Panel (b) shows the result of substituting absolute magnitude with stellar mass.

Table 4. Linear fits to the relations plotted in Figs 15 and 17.

	Slope	Intercept	Scatter
$\log\sigma_{\mathrm{V}}$ versus M_r	-0.125 ± 0.004	−0.464	0.073
$\log\sigma_{\mathrm{V}}$ versus $\log M_*$	0.286 ± 0.020	−0.895	0.071
$\log t_r$ versus $\log M_{\mathrm{dyn}}$	0.115 ± 0.056	8.628	0.085
$\log t_r$ versus $\log M_*$	0.112 ± 0.098	8.678	0.088
$\log Z$ versus $\log M_{\mathrm{dyn}}$	0.164 ± 0.010	−1.731	0.119
$\log Z$ versus $\log M_*$	0.168 ± 0.013	−1.757	0.122
$\Delta(\mathrm{Mgb}/\langle\mathrm{Fe}\rangle)$ versus $\log M_{\mathrm{dyn}}$	0.165 ± 0.012	−1.517	0.199
$\Delta(\mathrm{Mgb}/\langle\mathrm{Fe}\rangle)$ versus $\log M_*$	0.128 ± 0.013	−1.107	0.204

[13]We recall that the total stellar mass is obtained by multiplying the stellar mass-to-light ratio derived from a fit of the fibre spectrum by the total luminosity of the galaxy. This assumes that the stellar mass-to-light ratio outside the fibre is the same as that inside the fibre (see Paper I).

Table 5. Correlation between stellar and dynamical mass. The first two columns give the radius within which the dynamical mass is estimated and the slope of the velocity dispersion profile assumed to correct for aperture effects.

Radius	σ_V profile	ξ	Slope	Intercept	Scatter
$R_{50,r}$	−0.040	7.14	0.783 ± 0.019	2.19	0.127
$R_{50,r}$	−0.060	6.98	0.785 ± 0.021	2.18	0.128
$R_{50,r}$	−0.066	7.02	0.786 ± 0.017	2.17	0.128
$r_{\rm deV}$	−0.040	5.00	0.808 ± 0.026	1.93	0.113

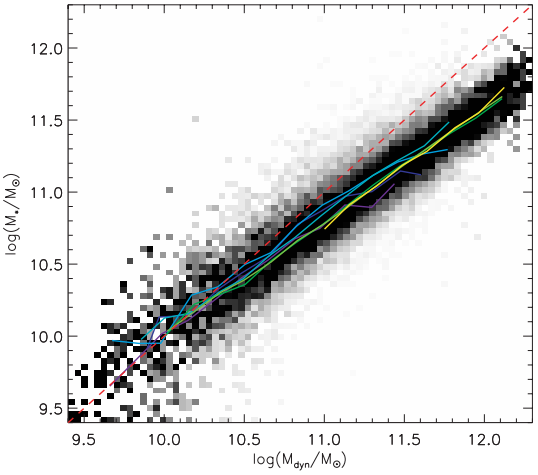

Figure 16. Relation between stellar mass and dynamical mass $M_{\rm dyn}$ estimated within the r-band Petrosian half-light radius (see equation 2). Lines of different colours represent the median relations in different bins of light-weighted age, increasing from $\log(t_r/{\rm yr}) = 9.5$ (purple) to 10.1 (yellow). The ratio between stellar and dynamical mass decreases with mass, as highlighted by the comparison with the one-to-one relation (dashed line).

because the zero-point is sensitive to our assumptions about the radius within which the dynamical mass is estimated, the conversion factor between dynamical and virial masses, and the stellar initial mass function (IMF; which we assume constant for all the galaxies). A linear fit to the relation in Fig. 16 yields

$$(M_*/{\rm M}_\odot) \propto (M_{\rm dyn}/{\rm M}_\odot)^{(0.783\pm0.019)} \quad (3)$$

with a scatter of 0.13 dex. The specific correction applied to σ_V has little effect on the fitted slope. As a check, we tried steeper velocity dispersion profiles, with slopes −0.06 (Mehlert et al. 2003) and −0.066 (Cappellari et al. 2006). These yielded relations between $\log M_*$ and $\log M_{\rm dyn}$ with slopes 0.785 ± 0.021 and 0.786 ± 0.017, respectively, i.e. consistent within 1σ with the slope of the relation in Fig. 16. We also tested the effect of estimating the dynamical mass within the effective de Vaucouleurs radius $r_{\rm deV}$ instead of $R_{50,r}$. The dynamical masses obtained in this case were systematically higher, by ∼0.13 dex, than those derived within $R_{50,r}$. The relation between $\log M_*$ and $\log M_{\rm dyn}$ had a slope of 0.808 ± 0.026, i.e. slightly higher but consistent within 1σ with the slope of the relation in Fig. 16. These results are summarized in Table 5.

A robust result from Fig. 16, therefore, is that the ratio between dynamical mass and stellar mass increases from the least massive to the most massive early-type galaxies in our sample. Structural non-homology does not appear to be responsible for this effect. We have built different subsamples of galaxies, based on the value of the Sersic index n fitted to the light profile in the SDSS data base. The slope of the relation between $\log M_*$ and $\log M_{\rm dyn}$ within each subsample remains close to that of the relation in Fig. 16, changing from 0.847 for $n = 3$ to 0.801 for $n = 5.5$ (a de Vaucouleurs profile corresponding to $n = 4$). Instead, the decrease in $M_*/M_{\rm dyn}$ with stellar mass in Fig. 16 is consistent with the increase in the dynamical mass-to-light ratio ($M_{\rm dyn}/L$) of early-type galaxies implied by the Fundamental Plane under the assumption of structural homology (Bender, Burstein & Faber 1992; Pierini et al. 2002; Zibetti et al. 2002; see also Cappellari et al. 2006, where no assumption on homology is made). This is also consistent with the increase in $M_{\rm dyn}/L$ with luminosity found by Padmanabhan et al. (2004) for a sample of 29 469 SDSS elliptical galaxies. The decrease of $M_*/M_{\rm dyn}$ with stellar mass could result from a more efficient mixing of dark matter and stars within the optical radius of massive galaxies relative to low-mass galaxies, as expected if the most massive early-type galaxies assembled through multiple mergers of dissipationless systems (see for discussion White 1980; Boylan-Kochlin, Ma & Quataert 2005; Humphrey et al. 2005; De Lucia et al. 2006).

The trend in $M_*/M_{\rm dyn}$ with stellar mass shows a weak dependence on galaxy light-weighted age. This is shown in Fig. 16, where lines of different colours indicate the median stellar mass as a function of dynamical mass for galaxies in various age bins, from $\log(t_r/{\rm yr}) = 9.5$ (purple) to 10.1 (yellow). Lines of constant age run parallel to the relation and, in spite of the small scatter, it appears that, at given dynamical mass, galaxies with more mass in stars are younger than those with small stellar mass (see also Fig. 15b). This weak trend cannot be accounted for entirely by the larger amount of mass returned to the interstellar medium by evolved stars in older galaxies relative to younger ones. For the Chabrier (2003) IMF adopted here, the returned stellar mass fraction of a simple stellar population increases by about 0.03 dex from $\log(t_r/{\rm yr}) = 9.5$ to 10 (with little dependence on metallicity; the differential change is similar for a Salpeter 1955 IMF). This effect can thus account for only about 10 per cent of the trend in $M_*/M_{\rm dyn}$ with age in Fig. 16.[14] The bulk of the trend might result from a systematically higher baryonic fraction and/or higher efficiency of conversion of baryons into stars in young early-type galaxies relative to old ones. For example, if many of our early types form by a merger of star-forming systems, those which currently have the youngest populations are presumably the most recently merged and so spent the longest time in the star-forming phase.

We now examine in more detail how age, stellar metallicity and α/Fe ratio depend on stellar and dynamical mass. This is shown in Fig. 17 for the early-type galaxies in our primary sample (Table 4 provides simple linear fits to the relations shown in the figure). The relations followed by age, metallicity and α/Fe ratio as a function of stellar mass (right-hand panels) reflect the conclusions drawn from our analysis of the CMR and Mg_2–σ_V relations in Sections 3.1 and 3.2. In particular, we find that light-weighted age increases (with a small scatter) with stellar mass in galaxies more massive than $10^{11}\,{\rm M}_\odot$, while there is a clear indication of a tail towards younger ages in less massive galaxies (Panel d; see also fig. 12 of Paper I). This confirms the results of several previous studies of smaller samples of early-type galaxies at low- and slightly higher redshifts (e.g. Caldwell & Rose 1998; Poggianti et al. 2001b; van Dokkum & Ellis 2003; Thomas et al. 2005; Treu et al. 2005). Stellar metallicity increases all the way from the least massive to the most massive galaxies in our sample (Panel e). The relation tends

[14] For example, at $M_{\rm dyn} \sim 10^{11}\,{\rm M}_\odot$, stellar mass increases from $\log M_*/{\rm M}_\odot \sim 10.75$ for $\log(t_r/{\rm yr}) = 10$ to ∼10.9 for $\log(t_r/{\rm yr}) = 9.5$.

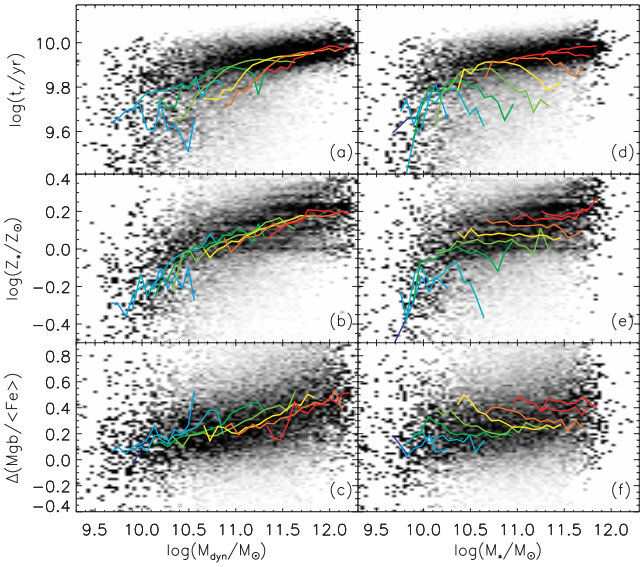

Figure 17. Left-hand panels: correlations between different physical parameters and the dynamical mass estimated within the *r*-band Petrosian half-light radius (see equation 2): (a) light-weighted age; (b) stellar metallicity; (c) α/Fe-estimator Δ (Mgb/$\langle$Fe$\rangle$). The grey-scale indicates the density of points at each location in the diagram, normalized to the total number of galaxies at fixed $\log(M_{\rm dyn}/{\rm M}_\odot)$. The solid lines represent the median relations for galaxies in different bins of stellar mass, centred on $\log(M_*/{\rm M}_\odot)$ = 9.6, 9.9, 10.2, 10.5, 10.8, 11.1, 11.4, 11.7 (increasing from blue to red). Right-hand panels: correlations between the same physical parameters and stellar mass. In this case, the solid lines represent the median relations for galaxies in different bins of dynamical mass, centred on $\log(M_{\rm dyn}/{\rm M}_\odot)$ = 9.6, 9.9, 10.2, 10.5, 10.8, 11.1, 11.4, 11.7, 12 (increasing from blue to red).

to steepen at stellar masses less than about $\sim 3 \times 10^{10}\,{\rm M}_\odot$, i.e. the characteristic mass scale of several observed bimodalities (see Paper I; Kauffmann et al. 2003; Baldry et al. 2004). We note that the dependence of stellar metallicity on stellar mass found here for early-type galaxies resembles quite closely the relation presented by Tremonti et al. (2004) for a sample of SDSS star-forming galaxies.

The increase in metallicity with stellar mass, and hence the CMR, is a natural prediction of different scenarios of early-type galaxy formation. In models in which the galaxies form monolithically in a single dissipationless collapse, star formation and chemical enrichment are generally assumed to be interrupted by the onset of galactic winds following the major episode of star formation. Since massive galaxies with deep potential wells are able to retain their gas for much longer times and so to reach higher metallicities than less massive galaxies, this scenario accounts for the CMR as a metallicity sequence (Larson 1974; Arimoto & Yoshii 1987; Bressan, Chiosi & Fagotto 1994; Tantalo et al. 1996). Early models of hierarchical galaxy formation neglected chemical enrichment and failed to produce sufficiently red, luminous elliptical galaxies (Kauffmann, White & Guiderdoni 1993; Cole et al. 1994). However, subsequent renditions of these models have been able to reproduce the observed slope and scatter of the CMR and of the Mg_2–$\sigma_{\rm V}$ relation by including chemical evolution and strong feedback even in massive galaxies together with metallicity-dependent population synthesis models (Kauffmann & Charlot 1998; De Lucia, Kauffmann & White 2004a). In this respect, the CMR of early-type galaxies does not represent a powerful tool to discriminate between the monolithic and merger formation scenarios (Kaviraj et al. 2005).

Additional clues about the formation of early-type galaxies may lie in their chemical abundance patterns. Fig. 17(f) shows that the α/Fe abundance ratio, as traced by the quantity Δ(Mgb/$\langle$Fe$\rangle$) (Section 2), increases linearly with $\log M_*$. This result, which was anticipated in several previous studies of early-type galaxies (Worthey et al. 1992; Greggio 1997; Jørgensen 1999), has been quantified using stellar population models with variable metal abundance ratios (Trager et al. 2000b; Mehlert et al. 2003; Thomas et al. 2005). If we consider as α enhanced those galaxies with Δ(Mgb/$\langle$Fe$\rangle$) > 0.2 (to account for the typical observational error on Mgb/$\langle$Fe$\rangle$), Fig. 17(f) indicates that early-type galaxies with solar abundance ratios are found only at $M_* \lesssim 10^{10.5}\,{\rm M}_\odot$, corresponding roughly to velocity dispersions $\sigma_{\rm V} \lesssim 100\,{\rm km\,s^{-1}}$. This is similar to the conclusion drawn by Kuntschner et al. (2001), based on the analysis of a sample of 72 early-type galaxies in groups and clusters.

The observed range in α/Fe abundance ratio and the increase of this ratio with stellar mass constitute a challenge for galaxy formation models. If the enrichment in α elements relative to iron reflects the star formation time-scale, as is assumed in standard chemical evolution models, the values Δ(Mgb/$\langle$Fe$\rangle$) > 0.2 found in high-mass early-type galaxies require star formation time-scales of the order 1–2 Gyr (see Section 4). Such short time-scales are plausible for the onset of galactic winds in the classical monolithic collapse scenario. Hierarchical models can also produce star formation histories which are peaked at high redshift for massive early-type galaxies, although subsequent star formation is expected at lower redshift in most models (Kauffmann 1996; Thomas 1999). A possible solution to this problem may be the suppression of late gas cooling (and hence star formation) by AGN-driven outflows in massive early-type galaxies. As shown by various recent models of hierarchical galaxy formation accounting for the combined effects of star formation and black hole accretion, the feedback provided by AGN can halt star formation on short time-scales (Granato et al. 2001, 2004; Springel, Di Matteo & Hernquist 2005; Croton et al. 2006; De Lucia et al. 2006). This mechanism is expected to be most effective in massive haloes hosting supermassive black holes, for which the time-scale to drive outflows could be as short as 1 Gyr (Granato et al. 2004). Hence, the increase in the α/Fe abundance ratio with stellar mass adds important constraints to models of early-type galaxy formation.

Fig. 17 also allows us to compare how age, metallicity and α/Fe ratio vary with dynamical mass (left-hand panels) versus stellar mass (right-hand panels). In the left-hand panels, lines of different colours show the median relations between each parameter and $M_{\rm dyn}$ followed by galaxies in different bins of stellar mass, increasing from $\log(M_*/{\rm M}_\odot) = 9.6$ to 11.7 in steps of $\sim$0.3 dex (from blue to red). In the right-hand panels, analogous lines show the median relations between each parameter and M_* followed by galaxies in different bins of dynamical mass. Fig. 17(d) shows that, at fixed dynamical mass, galaxies with large M_* tend to be younger than those with small M_* (in agreement with the result of Fig. 15b above). This trend is noticeable for dynamical masses in the range $10^{10} \lesssim M_{\rm dyn} \lesssim 10^{11.5}\,{\rm M}_\odot$. In contrast, at fixed dynamical mass, stellar metallicity is almost independent of M_* (Fig. 17e). In Fig. 17(f), galaxies with large M_* tend to have slightly lower Δ(Mgb/$\langle$Fe$\rangle$) and hence α/Fe than those with small M_* at fixed $M_{\rm dyn}$. This is consistent with the trend between Δ(Mgb/$\langle$Fe$\rangle$) and age identified in Fig. 18 below. A remarkable conclusion from the comparison between the right- and left-hand panels in Fig. 17 is that the chemical composition of early-type galaxies appears to depend primarily on dynamical mass rather than stellar mass.

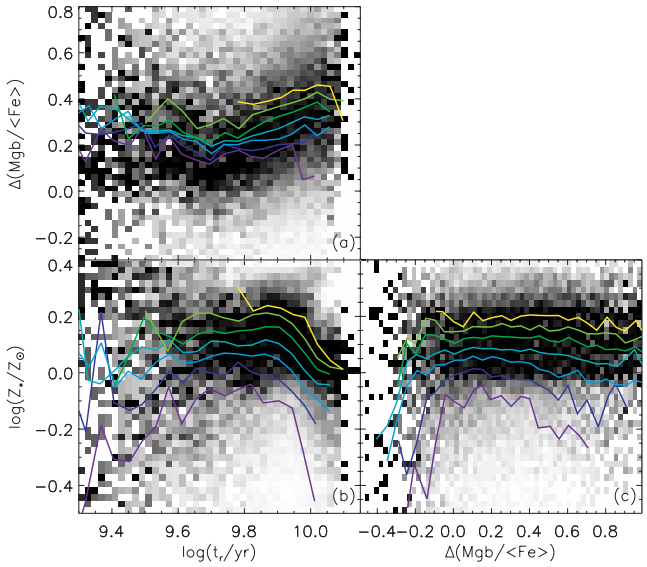

Figure 18. Correlations between stellar metallicity, light-weighted age and α/Fe-estimator $\Delta(\mathrm{Mgb}/\langle\mathrm{Fe}\rangle)$. The solid lines represent the median relations for galaxies in different bins of velocity dispersion, centred on $\log(\sigma_{\rm V}/\mathrm{km\,s^{-1}}) = 1.9, 2, 2.1, 2.2, 2.3, 2.4, 2.5$ (increasing from purple to yellow). The grey-scale indicates the density of galaxies with respect to the total at fixed abscissa.

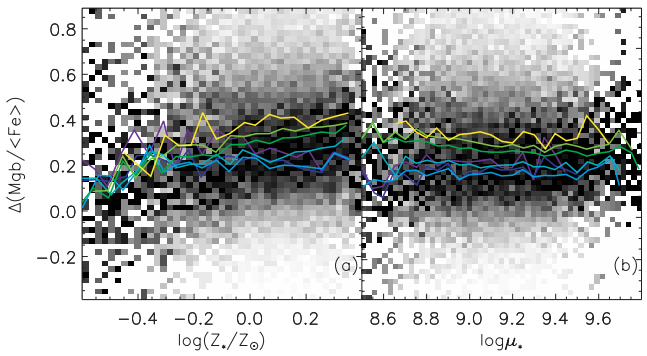

Figure 19. α/Fe-estimator $\Delta(\mathrm{Mgb}/\langle\mathrm{Fe}\rangle)$ plotted against (a) stellar metallicity and (b) surface stellar mass density within the r-band Petrosian half-light radius $R_{50,r}$. The solid lines represent the median relations for galaxies in different bins of light-weighted age, centred on $\log(t_r/\mathrm{yr}) = 9.5, 9.6, 9.7, 9.8, 9.9, 10, 10.1$ (increasing from purple to yellow).

It is also of interest to examine the relations between age, metallicity and α/Fe ratio. These are shown in Fig. 18 for our primary sample of early-type galaxies. In each panel, lines of different colours indicate the median trends followed by galaxies in different bins of velocity dispersion, from $\sigma_{\rm V} \sim 80$ km s^{-1} (purple) to $\sim$300 km s^{-1} (yellow). Fig. 18(b) shows that, at fixed velocity dispersion, age and metallicity are strongly anticorrelated for galaxies older than $\log(t_r/\mathrm{yr}) = 9.8$. Bernardi et al. (2005), who *assume* that the scatter about the CMR is caused entirely by age variations, suggest that young galaxies may be more metal rich than older galaxies at fixed velocity dispersion. Other previous studies also invoked an age–metallicity anticorrelation to explain the tightness of the colour–magnitude and the Mg_2–$\sigma_{\rm V}$ relations (e.g. Ferreras et al. 1999; Jørgensen 1999; Trager et al. 2000a; Terlevich & Forbes 2002, but see Kuntschner et al. 2001). However, the slope of this anticorrelation in Fig. 18(b) is consistent with the slope of the age–metallicity degeneracy for individual galaxies quantified in Paper I using the same sample of early-type galaxies. Thus, we cannot conclude here whether this anticorrelation is real or induced by correlated errors, but we note that the apparent scatter in age of massive, old ellipticals is consistent with the measurement error and the scatter in metallicity is quite small.

Fig. 18(c) shows the relation between $\Delta(\mathrm{Mgb}/\langle\mathrm{Fe}\rangle)$ and metallicity for the galaxies in our sample. Interestingly, even though both the colour–magnitude and the Mg_2–$\sigma_{\rm V}$ relations imply an increase in both total metallicity and α/Fe with mass, we do not identify any significant correlation between these two quantities (but see Fig. 19a below). This is true for the sample as a whole and for subsets of galaxies with fixed velocity dispersion. Instead, $\Delta(\mathrm{Mgb}/\langle\mathrm{Fe}\rangle)$ appears to correlate more strongly with light-weighted age for $\log(t_r/\mathrm{yr}) \gtrsim 9.7$, independent of galaxy velocity dispersion (Fig. 18a). Old galaxies appear to have larger α/Fe ratio than younger ones. This may be expected from the late enrichment in iron by Type Ia supernovae in galaxies which completed their star formation more recently, if the α/Fe ratio reflects the star formation time-scale. We might be tempted to relate star formation efficiency (and hence α enhancement) to stellar surface mass density, if the scaling between star formation rate and gas surface mass density in spiral galaxies can be extended to the progenitors of early-type galaxies (e.g. Schmidt 1959; Kennicutt 1998). Fig. 19(b) shows $\Delta(\mathrm{Mgb}/\langle\mathrm{Fe}\rangle)$ as a function of surface stellar mass density for the galaxies in our sample. The lines of different colours indicate the median trends followed by galaxies in different age bins, from $t_r \sim 3$ to 10 Gyr. We do not detect any significant correlation between $\Delta(\mathrm{Mgb}/\langle\mathrm{Fe}\rangle)$ and surface stellar mass density. For completeness, in Fig. 19(a), we show again $\Delta(\mathrm{Mgb}/\langle\mathrm{Fe}\rangle)$ as a function of metallicity, as in Fig. 18(c) (the grey-scale in this case indicates the distribution of galaxies as a function of $\Delta(\mathrm{Mgb}/\langle\mathrm{Fe}\rangle)$ at fixed metallicity). There appears to be a mild correlation between α/Fe and metallicity for galaxies in fixed age bins, in agreement with the results of Trager et al. (2000b).

4 SUMMARY AND CONCLUSIONS

We have analysed a sample of 26 003 early-type galaxies selected from the SDSS DR2 on the basis of their light concentration. Light-weighted ages, stellar metallicities and stellar masses for this sample were previously derived through the comparison of a set of carefully selected spectral absorption features with a comprehensive library of high-resolution population synthesis models, encompassing the full range of physically plausible star formation histories (paper I). In addition to these physical parameters, we have considered here an empirical estimate of the α-elements-to-iron abundance ratio, given by the offset $\Delta(\mathrm{Mgb}/\langle\mathrm{Fe}\rangle)$ between the observed ratio of the Mgb and $\langle$Fe$\rangle$ indices of a galaxy and that predicted by the best-fitting model in the library (which has scaled-solar abundance ratios). We have used these data to investigate the physical origin of two well-known scaling relations for early-type galaxies: the colour–magnitude and the Mg_2–$\sigma_{\rm V}$ relations.

Our analysis demonstrates unambiguously and with unprecedentedly good statistics that both the colour–magnitude and the Mg_2–$\sigma_{\rm V}$ relations are primarily sequences in galaxy stellar mass. At increasing stellar mass, as traced by either luminosity or velocity dispersion, the increasing colour and Mg-absorption line strength along the relations reflect an increase in both total metallicity and α/Fe ratio. Moreover, the galaxies in our sample cover a range in age of about 3–4 Gyr, with more massive galaxies being on average older than low-mass galaxies. While at high masses early-type galaxies

have the same mean age (and a small scatter in metallicity), at lower masses there is an increasing spread towards younger ages. This age spread dominates the scatter about the observed relations at low masses, in the sense that younger galaxies deviate towards bluer colours and lower Mg_2 index strengths than older galaxies of the same mass. These results are consistent with the conclusions from previous studies based on smaller samples of early-type galaxies (Kodama & Arimoto 1997; Colless et al. 1999; Vazdekis 2001; Worthey & Collobert 2003). In addition, we find that the scatter in metallicity at fixed stellar mass contributes significantly to the scatter about the two observational scaling relations, in particular at high masses.

We have checked that our main conclusions are not affected by possible dust effects and that they are robust against sample selection. In particular, the possible contamination of our sample by bulge-dominated star-forming galaxies, which could amount to $\sim$10 per cent, does not substantially affect on our results.

For a small subsample of 1765 galaxies, we used information on environmental density available from Kauffmann et al. (2004) to explore the dependence of the observed scaling relations and the stellar physical parameters on environment. We have found a small but detectable difference in the zero-point of the two relations, in the sense that early-type galaxies in dense environments tend to have redder colours and stronger Mg_2 absorption indices than galaxies in low-density regions, at fixed luminosity or velocity dispersion. We also find a systematic increase in the scatter about both relations from high to low densities. These variations appear to be induced by small differences in the light-weighted age and metallicity of galaxies located in different environments. While galaxies with similar mass have the same element abundance ratio regardless of environment, there is an increasing spread towards younger ages and lower metallicities in low-density environments. At fixed stellar mass, early-type galaxies in dense regions are on average 0.02-dex older and more metal rich than early-type galaxies in low-density regions. We note that these trends are very small and it will be worth re-examining them when a better statistics is available. If confirmed, these results are in agreement with previous studies indicating that early-type galaxies in clusters started to form stars earlier than, but on the same time-scale as early-type galaxies in the field (e.g. Thomas et al. 2005; Bernardi et al. 2006; Clemens et al. 2006).

We have also studied the dependence of the stellar mass on the dynamical mass estimated within the *r*-band Petrosian half-light radius of a galaxy. The relation is well described by a power law of exponent 0.783 ± 0.019 (equation 3), implying a decrease in the stellar-to-dynamical mass ratio from low- to high-mass galaxies. The correlations of physical parameters with the dynamical mass estimated in this way suggest that metallicity and element abundance ratios in early-type galaxies are more fundamentally related to dynamical mass than to stellar mass.

The increase in total metallicity with dynamical mass favours the classical interpretation of the colour–magnitude and Mg_2–σ_V relations in terms of supernova-driven winds (e.g. Trager et al. 2000a; Thomas et al. 2005). To account for the simultaneous increase in total metallicity and α/Fe ratio with mass, galactic winds should occur at early times, i.e. prior to the onset of Type Ia supernovae (on a time-scale of a few Gyr), which are the main contributors to Fe-peak elements. The winds will be more effective in removing α elements (produced by Type II supernovae on a time-scale of $\sim 10^8$ yr) from low-mass galaxies with shallow potential wells, while they should not reduce significantly the fraction of primordial gas and hence star formation (Mac Low & Ferrara 1999). Much observational evidence has been accumulated for the importance of galactic outflows in galaxies with masses up to at least $10^{10}\,M_\odot$ (Lehnert & Heckman 1996; Heckman et al. 2000; Pettini et al. 2000). Our results, if interpreted in terms of galactic winds, indicate that even more massive galaxies (with masses up to $\sim 10^{11}\,M_\odot$ in stars) have been affected by the ejection of metals through galactic winds.

The above scenario, however, cannot account alone for the observed values of α/Fe in early-type galaxies. In a galactic-wind scenario, massive galaxies are predicted to have solar α/Fe abundance ratios, while low-mass galaxies, which lose α elements at early times, should have lower than solar α/Fe ratios. Instead, galaxies with stellar masses less than about $3 \times 10^{10}\,M_\odot$ (corresponding to velocity dispersions less than $\sim$100 km s^{-1}) are observed to have nearly solar α/Fe ratios, while this ratio increases to supersolar values in more massive galaxies [the quantity $\Delta(\mathrm{Mgb}/\langle\mathrm{Fe}\rangle)$ reaching values around 0.3 in galaxies with stellar masses near $3 \times 10^{11}\,M_\odot$; see Fig. 17].

The supersolar α/Fe abundance ratios of massive early-type galaxies suggest that these formed on a relatively short time-scale and/or have/have had an IMF skewed towards high-mass stars. An IMF enriched in massive stars will produce a larger ratio of Type II to Type Ia supernovae, and hence a larger α/Fe ratio. Nagashima et al. (2005b) have shown that a top-heavy IMF during the burst ignited by the major merger that formed an elliptical galaxy can reproduce the observed range in α/Fe ratios. However, none of the models they explore yields the observed correlation of α/Fe with velocity dispersion (a model in which thermal conduction prevents the gas from cooling at the centres of massive haloes is able to produce an increase in the α-element abundance, but not the α/Fe ratio, with mass).

An interpretation of the α/Fe ratio in terms of the star formation time-scale is supported by the correlation we find between $\Delta(\mathrm{Mgb}/\langle\mathrm{Fe}\rangle)$ and light-weighted age, independent of mass (Fig. 18). This suggests that galaxies with longer star formation time-scales (and thus with more recently formed stellar populations) have lower α/Fe ratio than galaxies formed on shorter time-scales, because they had time to recycle the Fe-peak elements ejected by Type Ia supernovae. We also find that light-weighted age increases with stellar mass with negligible scatter at masses above $10^{11}\,M_\odot$ (Fig. 17d). Early-type galaxies less massive than about $\sim 10^{11}\,M_\odot$ display an extended tail towards younger ages, the mean age declining markedly with decreasing mass. This suggests either that low-mass galaxies formed more recently than high-mass galaxies, or that they have a more extended star formation history (consistent with their solar α/Fe ratios).

Our results represent further evidence for a shift in stellar growth towards less massive galaxies in recent epochs (Cowie et al. 1996; De Lucia et al. 2004b; Kodama et al. 2004; Treu et al. 2005; Yi et al. 2005). This 'downsizing' scenario may appear at odds with the expectations of original hierarchical models of galaxy formation. However, observations and the hierarchical paradigm can be reconciled if detailed physics of feedback from supernovae, AGN or thermal conduction is introduced (e.g. Benson et al. 2003; Granato et al. 2004; Nagashima et al. 2005a). These sources of feedback could inhibit star formation on time-scales short enough for the bulk of the star formation to be completed before Type Ia supernovae can substantially increase the iron abundance in massive galaxies. Springel et al. (2005) have shown that, in major mergers of spiral galaxies hosting supermassive black holes, AGN feedback provides a mechanism that can quench star formation on short time-scales. This mechanism is more efficient in the most massive early-type

galaxies and leaves dwarf spheroids almost unaffected. We also note that the short star formation time-scales (i.e. high formation redshifts) of massive early-type galaxies do not preclude longer assembly time-scales (De Lucia et al. 2006): massive early-type galaxies could appear old even if they assembled relatively recently. In this context, the new constraints derived here on the physical origin of the colour–magnitude and Mg_2–σ_V relations for early-type galaxies represent a valuable reference for future models.

ACKNOWLEDGMENTS

We thank Mariangela Bernardi for helpful discussion on sample selection and the anonymous referee for valuable suggestions that have improved our analysis. AG and SC thank the Alexander von Humboldt Foundation, the Federal Ministry of Education and Research and the Programme for Investment in the Future (ZIP) of the German Government for funding through a Sofja Kovalevskaja award. AG thanks the European Association for Research in Astronomy (EARA) training site and the European Community for a Marie Curie EST fellowship (MEST-CT-2004-504604). JB acknowledges the receipt of FCT fellowship BPD/14398/2003.

Funding for the creation and distribution of the SDSS Archive has been provided by the Alfred P. Sloan Foundation, the Participating Institutions, the National Aeronautics and Space Administration, the National Science Foundation, the US Department of Energy, the Japanese Monbukagakusho and the Max Planck Society. The SDSS website is http://www.sdss.org/. The Participating Institutions are the University of Chicago, Fermilab, the Institute for Advanced Study, the Japan Participation Group, the Johns Hopkins University, the Max Planck Institute for Astronomy (MPIA), the Max Planck Institute for Astrophysics (MPA), New Mexico State University, Princeton University, the United States Naval Observatory and the University of Washington.

REFERENCES

Abazajian K. et al., 2004, AJ, 128, 502
Abraham R. G. et al., 1996, ApJ, 471, 694
Arimoto N., Yoshii Y., 1987, A&A, 173, 23
Baldry I. K., Glazebrook K., Brinkmann J., Ivezić Ž., Lupton R. H., Nichol R. C., Szalay A. S., 2004, ApJ, 600, 681
Baldwin A., Phillips M. M., Terlevich R., 1981, PASP, 93, 817
Baum W. A., 1959, PASP, 71, 106
Bender R., Burstein D., Faber S. M., 1992, ApJ, 399, 462
Bender R., Burstein D., Faber S. M., 1993, ApJ, 411, 153
Benson A. J., Bower R. G., Frenk C. S., Lacey C. G., Baugh C. M., Cole S., 2003, ApJ, 599, 38
Bernardi M., Renzini A., da Costa L. N., Wegner G., Alonso M. V., Pellegrini P. S., Rité C., Willmer C. N. A., 1998, ApJ, 508, L143
Bernardi M. et al., 2003a, AJ, 125, 1817
Bernardi M. et al., 2003b, AJ, 125, 1849
Bernardi M. et al., 2003c, AJ, 125, 1866
Bernardi M. et al., 2003d, AJ, 125, 1882
Bernardi M., Sheth R. K., Nichol R. C., Schneider D. P., Brinkmann J., 2005, AJ, 129, 61
Bernardi M., Nichol R. C., Sheth R. K., Miller C. J., Brinkmann J., 2006, AJ, 131, 1288
Blakeslee J. P. et al., 2003, ApJ, 596, L143
Boylan-Kochlin M., Ma C.-P., Quataert E., 2005, MNRAS, 362, 184
Bower R. G., Lucey J. R., Ellis R. S., 1992, MNRAS, 254, 589
Bressan A., Chiosi C., Fagotto F., 1994, ApJS, 94, 63
Brinchmann J., Charlot S., White S. D. M., Tremonti C., Kauffmann G., Heckman T., Brinkmann J., 2004, MNRAS, 351, 1151
Bruzual G., Charlot S., 2003, MNRAS, 344, 1000
Burstein D., Davies R. L., Dressler A., Faber S. M., Lynden-Bell D., Terlevich R., Wegner G., 1988, in Audouze J., Pelletan M. C., Szalay A., eds, IAU Symp. 130, Large Scale Structures of the Universe. Kluwer, Dordrecht, p. 177
Caldwell N., Rose J. A., 1998, AJ, 115, 1423
Caldwell N., Rose J. A., Concannon K. D., 2003, AJ, 125, 2891
Cappellari M. et al., 2006, MNRAS, 366, 1126
Chabrier G., 2003, PASP, 115, 763
Clemens M. S., Bressan A., Nikolic B., Alexander P., Annibali F., Rampazzo R., 2006, preprint (astro-ph/0603714)
Cole S., Aragon-Salamanca A., Frenk C. S., Navarro J. F., Zepf S. E., 1994, MNRAS, 271, 781
Colless M., Burstein D., Davies R. L., McMahan R. K., Saglia R. P., Wegner G., 1999, MNRAS, 303, 813
Cowie L. L., Songaila A., Hu E. M., Cohen J. G., 1996, AJ, 112, 839
Croton D. J. et al., 2006, MNRAS, 365, 11
De Lucia G., Kauffmann G., White S. D. M., 2004a, MNRAS, 349, 1101
De Lucia G. et al., 2004b, ApJ, 610, L77
De Lucia G., Springel V., White S. D. M., Croton D., Kauffmann G., 2006, MNRAS, 366, 499
Denicoló G., Terlevich R., Terlevich E., Forbes D. A., Terlevich A., 2005, MNRAS, 358, 813
de Vaucouleurs G., 1961, ApJS, 5, 233
Djorgovski S., Davis M., 1987, ApJ, 313, 59
Faber S. M., 1973, ApJ, 179, 731
Faber S. M., Jackson R. E., 1976, ApJ, 204, 668
Ferreras I., Charlot S., Silk J., 1999, ApJ, 521, 81
Forbes D. A., Ponman T. J., 1999, MNRAS, 309, 623
Gallazzi A., Charlot S., Brinchmann J., White S. D. M., Tremonti C. A., 2005, MNRAS, 362, 41 (Paper I)
Gonzalez J. J., Faber S. M., Worthey G., 1993, BAAS, 25, 1355
Granato G. L., Silva L., Monaco P., Panuzzo P., Salucci P., De Zotti G., Danese L., 2001, MNRAS, 324, 757
Granato G. L., De Zotti G., Silva L., Bressan A., Danese L., 2004, ApJ, 600, 580
Greggio L., 1997, MNRAS, 285, 151
Guzman R., Lucey J. R., Carter D., Terlevich R. J., 1992, MNRAS, 257, 187
Heckman T. M., Lehnert M. D., Strickland D. K., Armus L., 2000, ApJS, 129, 493
Hogg D. W. et al., 2004, ApJ, 601, L29
Humphrey P. J., Buote D. A., Gastaldello F., Zappacosta L., Bullock J. S., Brighenti F., Mathews W. G., 2005, preprint (astro-ph/0510819)
Jørgensen I., 1999, MNRAS, 306, 607
Jørgensen I., Franx M., Kjaergaard P., 1996, MNRAS, 280, 167
Kauffmann G., 1996, MNRAS, 281, 487
Kauffmann G., Charlot S., 1998, MNRAS, 294, 705
Kauffmann G., White S. D. M., Guiderdoni B., 1993, MNRAS, 264, 201
Kauffmann G. et al., 2003, MNRAS, 341, 54
Kauffmann G., White S. D. M., Heckman T. M., Ménard B., Brinchmann J., Charlot S., Tremonti C., Brinkmann J., 2004, MNRAS, 353, 713
Kaviraj S., Devriendt J. E. G., Ferreras I., Yi S. K., 2005, MNRAS, 360, 60
Kennicutt R. C., 1998, ApJ, 498, 541
Kodama T., Arimoto N., 1997, A&A, 320, 41
Kodama T., Arimoto N., Barger A. J., Arag'on-Salamanca A., 1998, A&A, 334, 99
Kodama T., Bower R. G., Bell E. F., 1999, MNRAS, 306, 561
Kodama T. et al., 2004, MNRAS, 350, 1005
Kormendy J., 1977, ApJ, 218, 333
Korn A. J., Maraston C., Thomas D., 2005, A&A, 438, 685
Kuntschner H., Lucey J. R., Smith R. J., Hudson M. J., Davies R. L., 2001, MNRAS, 323, 615
Kuntschner H., Smith R. J., Colless M., Davies R. L., Kaldare R., Vazdekis A., 2002, MNRAS, 337, 172
Larson R. B., 1974, MNRAS, 166, 585
Larson R. B., Tinsley B. M., Caldwell C. N., 1980, ApJ, 237, 692
Lehnert M. D., Heckman T. M., 1996, ApJ, 462, 651
Mac Low M., Ferrara A., 1999, ApJ, 513, 142

Mehlert D., Thomas D., Saglia R. P., Bender R., Wegner G., 2003, A&A, 407, 423
Nagashima M., Lacey C. G., Baugh C. M., Frenk C. S., Cole S., 2005a, MNRAS, 358, 1247
Nagashima M., Lacey C. G., Okamoto T., Baugh C. M., Frenk C. S., Cole S., 2005b, MNRAS, 363, L31
Nelan J. E., Smith R. J., Hudson M. J., Wegner G. A., Lucey J. R., Moore S. A. W., Quinney S. J., Suntzeff N. B., 2005, ApJ, 632, 137
Padmanabhan N. et al., 2004, New Astron., 9, 329
Pettini M., Steidel C. C., Adelberger K. L., Dickinson M., Giavalisco M., 2000, ApJ, 528, 96
Pierini D., Gavazzi G., Franzetti P., Scodeggio M., Boselli A., 2002, MNRAS, 332, 422
Pimbblet K. A., Smail I., Kodama T., Couch W. J., Edge A. C., Zabludoff A. I., O'Hely E., 2002, MNRAS, 331, 333
Poggianti B. M. et al., 2001a, ApJ, 562, 689
Poggianti B. M. et al., 2001b, ApJ, 563, 118
Renzini A., 2006, preprint (astro-ph/0603479)
Salpeter E. E., 1955, ApJ, 121, 161
Schmidt M., 1959, ApJ, 129, 243
Schweizer F., Seitzer P., 1992, AJ, 104, 1039
Shimasaku K. et al., 2001, AJ, 122, 1238
Springel V., Di Matteo T., Hernquist L., 2005, MNRAS, 361, 776
Stanford S. A., Eisenhardt P. R., Dickinson M., 1998, ApJ, 492, 461
Strateva I. et al., 2001, AJ, 122, 1861
Tantalo R., Chiosi C., Bressan A., Fagotto F., 1996, A&A, 311, 361
Terlevich A. I., Forbes D. A., 2002, MNRAS, 330, 547
Terlevich A. I., Kuntschner H., Bower R. G., Caldwell N., Sharples R. M., 1999, MNRAS, 310, 445
Thomas D., 1999, MNRAS, 306, 655
Thomas D., Maraston C., Bender R., 2003, MNRAS, 339, 897
Thomas D., Maraston C., Korn A., 2004, MNRAS, 351, L19
Thomas D., Maraston C., Bender R., de Oliveira C. M., 2005, ApJ, 621, 673
Trager S. C., Faber S. M., Worthey G., González J. J., 2000a, AJ, 120, 165
Trager S. C., Faber S. M., Worthey G., González J. J., 2000b, AJ, 119, 1645
Tremonti C. A. et al., 2004, ApJ, 613, 898
Treu T., Ellis R. S., Liao T. X., van Dokkum P. G., 2005, ApJ, 622, L5
van Dokkum P. G., Ellis R. S., 2003, ApJ, 592, L53
Vazdekis A., 2001, Ap&SS, 276, 921
Vazdekis A., Kuntschner H., Davies R. L., Arimoto N., Nakamura O., Peletier R., 2001, ApJ, 551, L127
Visvanathan N., Sandage A., 1977, ApJ, 216, 214
White S. D. M., 1980, MNRAS, 191, 1P
Worthey G., 1994, ApJS, 95, 107
Worthey G., Collobert M., 2003, ApJ, 586, 17
Worthey G., Faber S. M., Gonzalez J. J., 1992, ApJ, 398, 69
Yi S. K. et al., 2005, ApJ, 619, L111
York D. G. et al., 2000, AJ, 120, 1579
Zibetti S., Gavazzi G., Scodeggio M., Franzetti P., Boselli A., 2002, ApJ, 579, 261

This paper has been typeset from a TEX/LATEX file prepared by the author.